6 Bentley, D. L. and Rabbits, T. H., Human immunoglobulin variable region genes – DNA sequences of two V kappa genes and a pseudogene. *Nature* 1980. 288: 730–733.

7 Moir, S., Lapointe, R., Malaspina, A., Ostrowski, M., Cole, C. E., Chun, T. W., Adelsberger, J. *et al.*, CD40-Mediated induction of CD4 and CXCR4 on B lymphocytes correlates with restricted susceptibility to human immunodeficiency virus type 1 infection: potential role of B lymphocytes as a viral reservoir. *J. Virol.* 1999. 73: 7972–7980.

8 Kuritzkes, D. R., Jacobson, J., Powderly, W. G., Godofsky, E., DeJesus, E., Haas, F., Reimann, K. A. *et al.*, Antiretroviral activity of the anti-CD4 monoclonal antibody TNX-355 in patients infected with HIV type 1. *J. Infect. Dis.* 2004. 189: 286–291.

9 Burastero, S. E., Gaffi, D., Lopalco, L., Tambussi, G., Borgonovo, B., De Santis, C., Abecasis, C. *et al.*, Autoantibodies to CD4 in HIV type 1-exposed seronegative individuals. *AIDS Res. Hum. Retroviruses* 1996. 12: 273–280.

10 Boon, L., Holland, B., Gordon, W., Liu, P., Shiau, F., Shanahan, W., Reimann, K. A. and Fung, M., Development of anti-CD4 MAb hu5A8 for treatment of HIV-1 infection: preclinical assessment in non-human primates. *Toxicology* 2002. 172: 191–203.

11 Shearer, M. H., Timanus, D. K., Benton, P. A., Lee, D. R. and Kennedy, R. C., Cross-clade inhibition of human immunodeficiency virus type 1 primary isolates by monoclonal anti-CD4. *J. Infect. Dis.* 1998. 177: 1727–1729.

12 Hurez, V., Kaveri, S. V., Mouhoub, A., Dietrich, G., Mani, J. C., Klatzmann, D. and Kazatchkine, M. D., Anti-CD4 activity of normal human immunoglobulin G for therapeutic use. (Intravenous immunoglobulin, IVIg). *Ther. Immunol.* 1994. 1: 269–277.

13 Bomsel, M., Pastori, C., Tudor, D., Alberti, C., Garcia, S., Ferrari, D., Lazzarin, A. and Lopalco, L., Natural mucosal antibodies reactive with first extracellular loop of CCR5 inhibit HIV-1 transport across human epithelial cells. *AIDS* 2007. 21: 13–22.

14 Sugden, B. and Mark, W., Clonal transformation of adult human leukocytes by Epstein–Barr virus. *J. Virol.* 1977. 23: 503–508.

15 Takekoshi, M., Maeda, F., Tachibana, H., Inoko, H., Kato, S., Takakura, I., Kenjyo, T. *et al.*, Human monoclonal anti-HCMV neutralizing antibody from phage display libraries. *J. Virol. Methods* 1998. 74: 89–98.

16 Takekoshi, M., Maeda, F., Nagatsuka, Y., Aotsuka, S., Ono, Y. and Ihara, S., Cloning and expression of human anti-tumor necrosis factor-alpha monoclonal antibodies from Epstein–Barr virus transformed oligoclonal libraries. *J. Biochem.* 2001. 130: 299–303.

17 Matsuda, F., Ishii, K., Bourvagnet, P., Kuma, K., Hayashida, H., Miyata, T. and Honjo, T., The complete nucleotide sequence of the human immunoglobulin heavy chain variable region locus. *J. Exp. Med.* 1998. 188: 2151–2162.

18 Huber, C., Schable, K. F., Huber, E., Klein, R., Meindl, A., Thiebe, R., Lamm, R. and Zachau, H. G., The V kappa genes of the L regions and the repertoire of V kappa gene sequences in the human germ line. *Eur. J. Immunol.* 1993. 23: 2868–2875.

19 Pech, M. and Zachau, H. G., Immunoglobulin genes of different subgroups are interdigitated within the VK locus. *Nucleic Acids Res.* 1984. 12: 9229–9236.

20 Healey, D., Dianda, L., Moore, J. P., McDougal, J. S., Moore, M. J., Estess, P., Buck, D. *et al.*, Novel anti-CD4 monoclonal antibodies separate human immunodeficiency virus infection and fusion of CD4+ cells from virus binding. *J. Exp. Med.* 1990. 172: 1233–1242.

21 Peterson, A. and Seed, B., Genetic analysis of monoclonal antibody and HIV binding sites on the human lymphocyte antigen CD4. *Cell* 1988. 54: 65–72.

22 Benkirane, M., Hirn, M., Carriere, D. and Devaux, C., Functional epitope analysis of the human CD4 molecule: antibodies that inhibit human immunodeficiency virus type 1 gene expression bind to the immunoglobulin CDR3-like region of CD4. *J. Virol.* 1995. 69: 6898–6903.

23 Sattentau, Q. J., Dalgleish, A. G., Weiss, R. A. and Beverley, P. C., Epitopes of the CD4 antigen and HIV infection. *Science* 1986. 234: 1120–1123.

24 Pal, R., Nair, B. C., Hoke, G. M., Sarngadharan, M. G. and Edidin, M., Lateral diffusion of CD4 on the surface of a human neoplastic T-cell line probed with a fluorescent derivative of the envelope glycoprotein (gp120) of human immunodeficiency virus type 1 (HIV-1). *J. Cell. Physiol.* 1991. 147: 326–332.

25 Finnegan, C. M., Rawat, S. S., Cho, E. H., Guiffre, D. L., Lockett, S., MerrillJr., A. H. and Blumenthal, R., Sphingomyelinase restricts the lateral diffusion of CD4 and inhibits human immunodeficiency virus fusion. *J. Virol.* 2007. 81: 5294–5304.

26 Rawat, S. S., Zimmerman, C., Johnson, B. T., Cho, E., Lockett, S. J., Blumenthal, R. and Puri, A., Restricted lateral mobility of plasma membrane CD4 impairs HIV-1 envelope glycoprotein mediated fusion. *Mol. Membr. Biol.* 2008. 25: 83–94.

27 Xavier, R., Brennan, T., Li, Q., McCormack, C. and Seed, B., Membrane compartmentation is required for efficient T cell activation. *Immunity* 1998. 8: 723–732.

28 Millan, J., Cerny, J., Horejsi, V. and Alonso, M. A., CD4 segregates into specific detergent-resistant T-cell membrane microdomains. *Tissue Antigens* 1999. 53: 33–40.

29 Nguyen, D. H., Giri, B., Collins, G. and Taub, D. D., Dynamic reorganization of chemokine receptors, cholesterol, lipid rafts, and adhesion molecules to sites of CD4 engagement. *Exp. Cell. Res.* 2005. 304: 559–569.

30 Maeda, F., Nagatsuka, Y., Ihara, S., Aotsuka, S., Ono, Y., Inoko, H. and Takekoshi, M., Bacterial expression of a human recombinant monoclonal antibody fab fragment against hepatitis B surface antigen. *J. Med. Virol.* 1999. 58: 338–345.

31 Shimizu, S., Urano, E., Futahashi, Y., Miyauchi, K., Isogai, M., Matsuda, Z., Nohtomi, K. *et al.*, Inhibiting lentiviral replication by HEXIM1, a cellular negative regulator of the CDK9/cyclin T complex. *AIDS* 2007. 21: 575–582.

32 Nagatsuka, Y., Hara-Yokoyama, M., Kasama, T., Takekoshi, M., Maeda, F., Ihara, S., Fujiwara, S. *et al.*, Carbohydrate-dependent signaling from the phosphatidylglucoside-based microdomain induces granulocytic differentiation of HL60 cells. *Proc. Natl. Acad. Sci. USA* 2003. 100: 7454–7459.

Abbreviations: **B-LCL:** B-lymphoblastoid cell lines · **rhCD4:** recombinant human CD4 · **sHM:** somatic hypermutation

Full correspondence: Dr. Jun Komano, AIDS Research Center, National Institute of Infectious Diseases, 1-23-1 Shinjuku, Tokyo 162-864, Japan
Fax: +81-3-5285-1111
e-mail: ajkomano@nih.go.jp

Additional correspondence: Dr. Masataka Takekoshi, Department of Molecular Life Science, Division of Basic Molecular Science and Molecular Medicine, Tokai University School of Medicine, Isehara, Japan
E-mail: mtakekos@is.icc.u-tokai.ac.jp

Received: 2/4/2009
Revised: 22/12/2009
Accepted: 1/2/2010

Dominant-negative derivative of EBNA1 represses EBNA1-mediated transforming gene expression during the acute phase of Epstein–Barr virus infection independent of rapid loss of viral genome

Yumi Kariya,[1,2] Makiko Hamatake,[1] Emiko Urano,[1] Hironori Yoshiyama,[3] Norio Shimizu[2] and Jun Komano[1,4]

[1]AIDS Research Center, National Institute of Infectious Diseases, Tokyo; [2]Department of Virology, Division of Medical Science, Medical Research Institute, Tokyo Medical and Dental University, Tokyo; [3]Research Center for Infection-associated Cancer, Institute for Genetic Medicine, Hokkaido University, Sapporo, Japan

(Received November 1, 2009/Revised November 30, 2009/Accepted December 6, 2009)

The oncogenic human herpes virus, the Epstein–Barr virus (EBV), expresses EBNA1 in almost all forms of viral latency. EBNA1 plays a major role in the maintenance of the viral genome and in the transactivation of viral transforming genes, including EBNA2 and latent membrane protein (LMP-1). However, it is unknown whether inhibition of EBNA1 from the onset of EBV infection disrupts the establishment of EBV's latency and transactivation of the viral oncogenes. To address this, we measured EBV infection kinetics in the B cell lines BALL-1 and BJAB, which stably express a dominant-negative EBNA1 (dnE1) fused to green fluorescent protein (GFP). The EBV genome was surprisingly unstable 1 week post-infection: the average loss rate of EBV DNA from GFP- and GFP-dnE1-expressing cells was 53.4% and 41.0% per cell generation, respectively, which was substantially higher than that of an 'established' *oriP* replicon (2–4%). GFP-dnE1 did not accelerate loss of the EBV genome, suggesting that EBNA1-dependent licensing of the EBV genome occurs infrequently during the acute phase of EBV infection. In the subacute phase, establishment of EBV latency was completely blocked in GFP-dnE1-expressing cells. In contrast, C/W promoter-driven transcription was strongly restricted in GFP-dnE1-expressing cells at 2 days post-infection. These data suggest that inhibition of EBNA1 from the onset of EBV infection is effective in blocking the positive feedback loop in the transactivation of viral transforming genes, and in eradicating the EBV genome during the subacute phase. Our results suggest that gene transduction of GFP-dnE1 could be a promising therapeutic and prophylactic approach toward EBV-associated malignancies. (*Cancer Sci* 2010)

The Epstein–Barr virus (EBV) is a risk factor in several malignant diseases including Burkitt's lymphoma and nasopharyngeal carcinoma.[1–4] The opportunistic B-cell lymphoma is becoming the major cause of death in AIDS patients in an era of highly active antiretroviral therapy (HAART), and EBV is associated with a significant portion of AIDS lymphoma cases.[5,6] Neither an EBV vaccine, nor specific antiviral agents against EBV are available; thus attention should be paid to the development of therapeutic agents against EBV.

EBV-encoded genes including EBNA1, EBNA2, and latent membrane protein (LMP-1) are potential molecular targets for the treatment of EBV-associated lymphomas because they play central roles in the process of malignant transformation.[7] We are interested in EBNA1 since it contributes to EBV oncogenesis in two ways: it supports the maintenance of the EBV genome in *cis* and enhances expression of viral oncogenes, including EBNA2 and LMP-1, in *trans*.[7–9] EBNA1 exerts its biological functions by binding to its cognate binding sites within the family of repeats (FR) and the dyad symmetry element (DS) located within the origin of replication (oriP) of EBV DNA. EBNA1 interacts with FR to enhance transcription from the viral C/W promoters (C/Wp) and to partition EBV DNA to daughter cells; and with DS to initiate DNA replication.[7–9]

Maintenance of the oriP replicon is stable once EBV latency has been established. The loss rate of established oriP plasmids is estimated at 2–4% per cell generation.[10,11] Interestingly, the loss rate of the oriP replicon is significantly higher in cells transiently transduced with oriP plasmids (>25% per cell generation) than in established cells.[12] In primary B cells, EBV DNA is lost rapidly within 2 days post-infection (~98.9%).[13] However, the loss rate of the EBV genome during a week post-infection in B cells remains to be quantified.

Upon EBV infection, the first viral genes expressed are the transactivators EBNA2 and EBNA-LP transcribed from Wp several hours after infection.[7] EBNA2 binds to the EBNA2-responsive elements and, in cooperation with EBNA-LP, enhances transcription from Cp, which leads to expression of all EBNA proteins, including EBNA1. EBNA1 binding to oriP activates C/Wp to boost viral latent gene expression, including the EBNAs and LMP-1. The viral gene transactivation positive feedback loop is established within a few days post-infection, and EBNA1 is one of the key factors that sustain this feedback loop during the acute phase of EBV infection.[14] In parallel, EBNA1 contributes to the establishment of the EBV genome as a licensed replicon. It may be possible to stop EBV infection by breaking the chain of EBNA1-dependent events and thus the EBV-mediated malignant transformation of infected cells. Previous studies have assessed the therapeutic potential of a dominant-negative derivative of EBNA1 (dnE1) in cells in which EBV latency was already established.[15,16] In this study, we critically assessed whether inhibition of EBNA1 limits the early stage of EBV infection in B cells. We provide evidence that expression of dnE1 strongly blocks the expression of virus-encoded oncogenes in acutely infected cells without accelerating EBV genome loss, and disrupts EBV latency in the subacute phase of EBV infection.

Materials and Methods

Cells. The 293T, EBV-negative Burkitt lymphoma cell line BJAB, EBV-positive Burkitt lymphoma cell line Daudi, EBV-transformed healthy donor-derived B lymphoblastoid cell line (B-LCL), and B acute lymphoblastic leukemia cell line BALL-1

[4]To whom correspondence should be addressed.
E-mail: ajkomano@nih.go.jp

doi: 10.1111/j.1349-7006.2009.01474.x

cells (kindly provided by Dr. Yokota, National Institute of Infectious Diseases, Tokyo, Japan) were maintained in RPMI-1640 medium (Sigma, St. Louis, MA, USA) supplemented with 10% fetal bovine serum (Japan Bioserum, Tokyo, Japan), 50 U/mL penicillin, 50 μg/mL streptomycin (Invitrogen, Tokyo, Japan), and incubated at 37°C in a humidified 5% CO_2 atmosphere.

Plasmids. The following primers were used to amplify dnE1 from p1160[17] by PCR: 5′-ACCGGTCTCGAGCAATTGCCA-CCATGCGGGGTCAGGGTGATGGAGG-3′ and 5′-GGATC-CTCGAGCGGCCGCTCACTCCTGCCCTTCCTCACC-3′. The GFP-dnE1 expression vector (pGD) was constructed by cloning the MfeI-XhoI fragment of the PCR product into the BglII-SalI sites of pEGFP-C1 (Clontech, Palo Alto, CA, USA). The MfeI and BglII sites were blunted with T7 RNA polymerase. The AgeI-BamHI fragment from pGD was cloned into the corresponding restriction sites of pCMMP eGFP[15,18] to generate pCMMP GFP-dnE1. The EBNA1 expression vector p1553, the FR-tk-luciferase reporter p985, and pLuciferase (pCMV-luc) have been described previously.[17–20]

Luciferase assay. The 293T cells, grown in 48-well plates, were co-transfected with the indicated plasmids using Lipofectamine 2000 according to the manufacturer's protocol (Invitrogen, Tokyo, Japan). Cells were replated in 96-well plates in triplicate at 2 h post-transfection. Luciferase activity was measured 48 h after transfection using the Steady-Glo Kit (Promega, Madison, WI, USA).

Murine leukemia virus (MLV) vector infection and cell sorting. MLV vectors were produced as described previously.[18] B cells (1×10^7 cells) were incubated with 2 mL of MLV preparation overnight at 4°C with continuous agitation. GFP-positive cells were collected using a FACS sorter (FACS Vantage; Becton Dickinson, San Jose, CA, USA) at 11 days post-infection.

Western blotting. Western blotting was performed as described previously.[21,22] The following reagents were used: anti-GFP (MsX Green Fluorescent Protein; Chemicon, Temecula, CA, USA) and Envision$^+$ Dual Link System-HRP (Dako, Glostrup, Denmark).

EBV infection and nucleic acid extraction. The EBV B95-8 strain was a generous gift from Dr Fujiwara's group at the National Research Institute for Child and Development (Tokyo, Japan). B cells (1×10^7 cells) were incubated with 100 μL of B95-8 EBV for 1 h at 37°C, and genomic DNA was extracted from half of the infected cells soon after infection (QIAamp DNA Mini Kit; Qiagen, Tokyo, Japan). At 15 h post-infection, half of the cells were washed once with PBS and incubated for 5 min in lysis buffer (10 mM Tris-HCl [pH7.4], 10 mM NaCl, 3 mM $MgCl_2$, and 0.5% NP-40). The nuclear fraction was collected by centrifugation for 5 min at 20.6 K × *g* (Kubota 3740; Kubota, Tokyo, Japan), and high molecular weight DNA was extracted (nuclear DNA). At 2 days post-infection and at later time points, high molecular weight DNA, or total RNA (PureLink Total RNA Blood Purification Kit; Invitrogen) was extracted from 1×10^6 or 3×10^6 cells, respectively, according to the manufacturer's protocol. After EBV infection, 10 μM aciclovir (Kayaku, Tokyo, Japan) was added to the culture medium. The production and infection of the recombinant EBV Akata strain carrying GFP and neomycin resistant genes has been described previously.[23] At 2 days post-infection, cells were plated at a density of 1×10^4 cells per well in a flat-bottomed 96-well plate, and cultured in a medium containing 1 mg/mL G418. The efficiency of EBV latency establishment was evaluated as percentage of wells positive for the emergence of G418-resistant cells at 2 to 3 weeks post-G418 selection.

Quantitative real-time PCR. Real-time PCR was performed as described previously; serial dilutions of positive controls were used as standards.[21] Amplifications were performed using the QuantiTect SYBR Green RT-PCR/PCR Kit (Qiagen), and the following primers: BamHI W repeat, 5′-GCCAGAGG-TAAGTGGACTTT-3′ and 5′-AGAAGCATGTATACTAAGC-CTCCC-3′; cyclophilin A (CYPA), 5′-CACCGCCACCATG-GTCAACCCCA-3′ and 5′-CCCGGGCCTCGAGCTTTCGAG-TTGTCCACAGTCAGCAATGG-3′; C/Wp, 5′-CCCTCGGA-CAGCTCCTAAG-3′ and 5′-CTTCACTTCGGTCTCCCCTA-3′; EBER1, 5′-AAAACATGCGGACCACCAGC-3′ and 5′-AG-GACCTACGCTGCCCTAGA-3′. The β-globin primers were described previously.[21] Following PCR amplification, the amplicons were separated in a 2% agarose gel, stained with ethidium bromide, and imaged with a Typhoon scanner (GE Healthcare Bio-Sciences; Piscataway, NJ, USA).

Results

Construction and functional verification of dnE1 fused to GFP. The carboxy half of EBNA1 serves as a functional dominant-negative inhibitor of EBNA1 that restricts the replication and maintenance of oriP plasmids as well as the EBNA1-dependent enhancement of transcription.[17,24] We used a dnE1 mutant encompassing amino acids 377 to 391 (the nuclear localization signal, NLS) and 451 to 641 (the DNA binding and dimerization domain) of EBNA1 (Fig. 1A).[17] To visualize the intracellular distribution of dnE1, we constructed the retroviral expression vector encoding GFP-dnE1. The expression of GFP-dnE1 was verified in transiently transfected 293T cells and stably transduced B cell lines using an MLV vector. To verify the function of GFP-dnE1, we conducted a reporter assay using a plasmid encoding the FR-tk-luciferase cassette. EBNA1 enhances expression of FR-tk-luciferase by binding to FR. If the GFP-dnE1 construct retains dnE1 function, co-expressing EBNA1 and GFP-dnE1 should reduce reporter activity. Luciferase activity was increased significantly upon EBNA1 expression by approximately 5.3-fold, consistent with previous findings (Fig. 1B, $P < 0.05$, two-tailed Student's *t*-test).[17] When GFP-dnE1 was co-expressed, the luciferase activity was decreased. The decrease in luciferase activity was proportional to the increase in GFP-dnE1 expression vector (Fig. 1B, maximum reduction: 22.3%, $P < 0.05$, two-tailed Student's *t*-test). This effect was not observed with GFP alone. In addition, CMV promoter-driven luciferase expression was unaffected by EBNA1, GFP-dnE1, and GFP, suggesting that the reduction in luciferase activity with GFP-dnE1 in the EBNA1/FR-tk-luciferase system is specific. These data indicate that GFP-dnE1 functions as an inhibitor of EBNA1.

Establishment of B cells constitutively expressing GFP-dnE1. To investigate the potential effect of GFP-dnE1 on EBV infection in B cells, we established BALL-1 and BJAB cells, which constitutively express GFP-dnE1, using an MLV vector. GFP was used as a control throughout this study. The distribution of GFP-dnE1 was examined by confocal microscopy, which revealed an even distribution of GFP throughout the cell. In contrast, the majority of GFP-dnE1was localized to the nucleus due to the presence of the NLS (Fig. 2A). Similar observations were made in BJAB and 293T cells (data not shown). We sorted the GFP- or GFP-dnE-expressing cells using a FACS sorter. To test the dose-dependent effect, we collected BALL-1 cell populations bearing high or low levels of GFP fluorescence, denoted as Hi and Lo, respectively. The expression of GFP and GFP-dnE1 was verified by Western blotting, which confirmed that GFP and GFP-dnE1 Hi cells had higher intensity signals than the GFP and GFP-dnE1 Lo cells (Fig. 2B). The rate of cell proliferation and the morphology of GFP-dnE1 cells were indistinguishable from those of GFP cells (Fig. 2A and data not shown).

Effect of GFP-dnE1 on the nuclear translocation of EBV DNA during the acute phase of EBV infection. To assess whether GFP-dnE1 could restrict the nuclear targeting of the EBV

doi: 10.1111/j.1349-7006.2009.01474.x

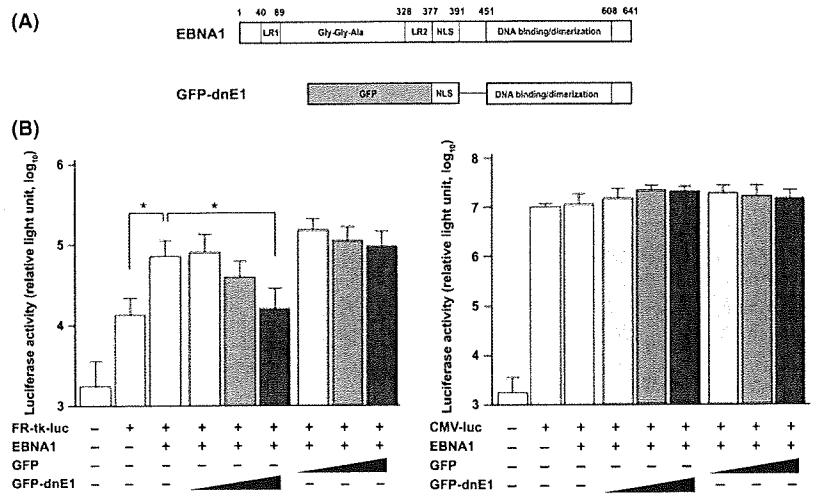

Fig. 1. Construction and functional characterization of a dominant-negative EBNA1 mutant (dnE1) fused to green fluorescent protein (GFP). (A) Structure of the EBNA1 protein and dnE1 used in this study. The linking regions (LR1 and LR2), the Gly-Gly-Ala repeat, the nuclear localization signal (NLS), and the DNA binding and dimerization domain are shown. GFP-dnE1 encodes the NLS and DNA binding and dimerization domain of EBNA1 fused to the C-terminus of GFP. (B) Repression of EBNA1-dependent transcriptional activation by GFP-dnE1. We transfected 293T cells in 48-well plates with 200 ng of FR-tk-luc or CMV-luc reporter, and 500 ng of EBNA1 expression vector, along with increasing amounts of GFP or GFP-dnE1 expression vector (20, 100, and 500 ng, respectively). $*P < 0.05$, two-tailed Student's *t*-test.

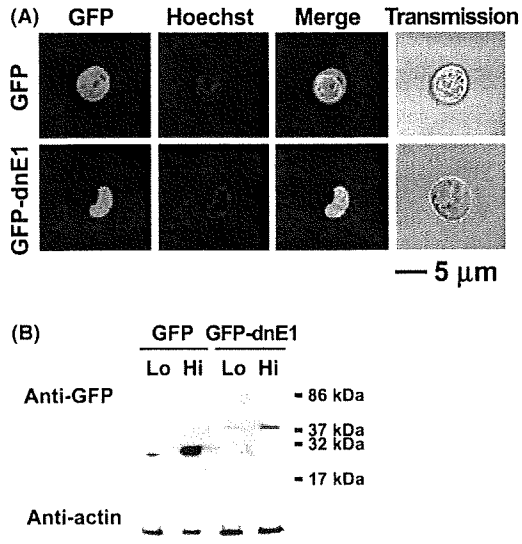

Fig. 2. Verification of stable green fluorescent protein (GFP)-dominant-negative EBNA1 (dnE1) expression in BALL-1 cells. (A) Distribution of GFP and GFP-dnE1 in BALL-1 cells was examined by confocal microscopy. Cells were imaged unfixed using a confocal microscope META 510 (Carl Zeiss, Tokyo, Japan). The green signal represents GFP fluorescence, and blue represents the Hoechst-stained nucleus. The bar represents 5 μm; magnification, ×630. (B) GFP or GFP-dnE1 expression in stably transduced BALL-1 cells was examined by Western blot analysis using an anti-GFP antibody. Protein lysates from 5×10^5 cells were loaded for each sample, except GFP Hi cells (5×10^4). The molecular weight marker is shown on the right.

genome after infection, we measured the amount of EBV DNA recovered from cells immediately after infection (representing the amount of EBV attached to cells) and the amount of EBV DNA that had migrated into the nucleus at 1 day post-infection. We isolated the nuclear fraction to exclude EBV DNA that failed to enter the nucleus. The number of EBV DNA molecules per cell was estimated by real-time PCR, which targeted the BamHI W repeat, in 10 ng of genomic DNA. We estimated the number of EBV DNA per cell given that a single cell contains approximately 10 pg of genomic DNA, and an EBV DNA has 10 copies of BamHI W repeats on average. The nuclear targeting efficiencies of EBV DNA were as follows: BALL-1 GFP cells, 43.3–108.6%; GFP-dnE1 cells, 46.9–65.6%; BJAB GFP cells, 37.4%; GFP-dnE1 cells, 35.0% (Table 1). These data suggested that the effect of GFP-dnE1 on the nuclear targeting of EBV DNA should be assessed more sensitively in BALL-1 and BJAB cell systems than in primary B cells because the nuclear targeting efficiency of EBV DNA in primary B cells is extremely inefficient (~1.1%).[13] In our experimental systems, the nuclear targeting efficiencies of EBV DNA in GFP-dnE1-expressing cells were similar to those in GFP-expressing cells. In addition, the dose-dependency of GFP-dnE1 was not observed in BALL-1 cells (Table 1). These data suggest that the nuclear targeting efficiency of EBV DNA was not restricted by the presence of GFP-dnE1 in B cells upon EBV infection.

Effect of GFP-dnE1 on the rate of loss of EBV DNA during the acute phase of EBV infection. To examine the effect of GFP-dnE1 on the rate of loss (ROL) of EBV DNA during the acute phase of viral infection, we monitored the EBV DNA copy number from day 2 to day 5 or day 6 post-infection, by real-time PCR, which detects the viral genome in both linear and circular configurations (Table 1). The ROL was estimated as the percentage reduction of EBV DNA per cell generation, considering that the cell doubling time is 24 h, and the kinetics of viral genome loss follows an exponential decay. The ROL in GFP-dnE1-expressing cells (19.2–85.9% per cell generation) was similar to GFP-expressing cells (20.5–79.4% per cell generation) in both BALL-1 and BJAB cells. In addition, there was no detectable dose-dependent effect of GFP-dnE1 in BALL-1 cells (Table 1 and Fig. 3). The averages ± SEs of ROL in GFP- and GFP-dnE1-expressing cells from six independent measurements in BALL-1 cells were 37.7 ± 10.7% and 25.7 ± 6.5% per cell generation, respectively (data not shown), which was substantially higher than the rate of loss of an established oriP replicon (2–4%).[10,11] These results reflect the precipitous loss of oriP plas-

Table 1. The kinetics of EBV DNA in the acute phase of EBV infection

Cell	Copy number of EBV DNA per cell at the indicated day†				Nuclear transport (%‡)	Rate of loss of EBV DNA (% per cell generation§)
Expt 1						
BALL-1	Day 0	Day 1	Day 2	Day 5		
GFP Hi	20.38	11.92	3.57	0.01¶	58.5	85.9
GFP Lo	17.26	11.68	3.21	0.56	67.7	44.1
GFP-dnE1 Hi	23.02	10.79	3.30	0.30	46.9	54.9
GFP-dnE1 Lo	18.83	12.36	1.46	0.53	65.6	28.7
BJAB	Day 0	Day 1	Day 2	Day 5		
GFP	155.1	58.8	5.38	0.06	37.4	77.7
GFP-dnE1	64.6	37.4	5.69	0.05	58.0	79.4
Expt 2						
BALL-1	Day 0	Day 1	Day 2	Day 6		
GFP Hi	16.33	17.73	11.10	4.74	108.6	19.2
GFP Lo	17.35	7.51	8.75	1.13	43.3	40.1
GFP-dnE1 Hi	18.46	8.71	8.95	3.38	47.2	21.6
GFP-dnE1 Lo	14.14	7.05	6.97	2.79	49.9	20.5

†Nuclear DNA was used for day 1 data. ‡Estimated from day 0 and day 1 data. §Estimated from day 2 and day 5 or day 6 data with the exponential decay. ¶Below the limit of detection. dnE1, dominant-negative EBNA1; EBV, Epstein–Barr virus; GFP, green fluorescent protein.

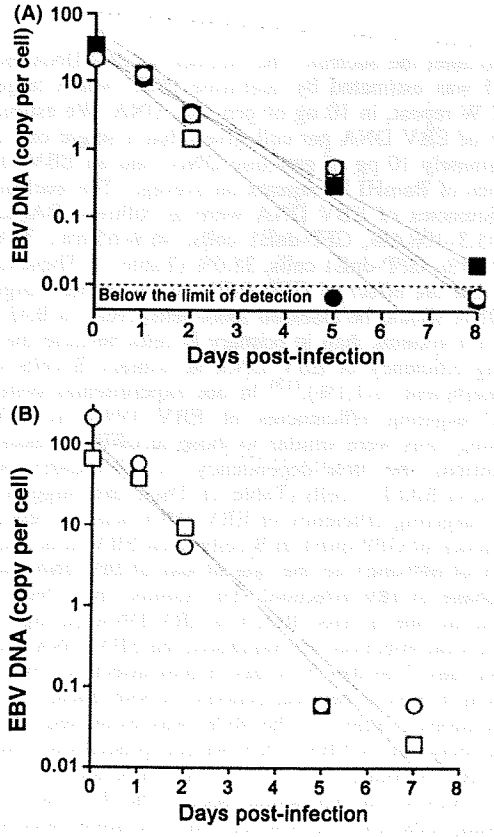

Fig. 3. Kinetics of Epstein–Barr virus (EBV) DNA loss during the acute phase of EBV infection. (A) Representative data from BALL-1 cells (Expt. 1 in Table 1) is shown. The filled squares, open squares, filled circles, and open circles represent GFP Hi, GFP Lo, GFP-dnE1 Hi, and GFP-dnE1 Lo, respectively. The limit of detection was below 0.01 (dashed line). The gray lines represent an approximation to the exponential decay. The dashed gray line represents the 4% rate of loss per cell generation. (B) Representative data from BJAB cells shown in Table 1. The circles and squares represent GFP and GFP-dnE1, respectively. Please see Table 1 for the detailed analysis.

mids (26–37%) in transiently transfected non-B cells.[12] The data suggest that GFP-dnE1 is unable to accelerate the ROL in the acute phase of EBV infection in B cells, presumably because the EBV genome is not established as an EBNA1-dependent stable licensed replicon. It should be noted that this is the first time that quantitative ROL data has been obtained by introducing the oriP replicon into B cells via EBV infection, which is an approach that does not confer any selective advantage on the infected cells.

Effect of GFP-dnE1 on efficiency of establishment of EBV latency. Cells infected with recombinant EBV, carrying the neomycin resistance gene, were seeded at 5×10^3 cells per well into a 96-well plate, and the efficiency of the establishment of EBV latency was assessed as the percentage of wells positive for the emergence of G418-resistant cells. G418-resistant cells appeared in BJAB, Daudi, parental BALL-1, and BALL-1 GFP cells at 56–100% efficiencies. In sharp contrast, G418-resistant cells were absent from GFP-dnE1-expressing BALL-1 cells (Table 2). These data clearly suggest that, although the ROL during the acute phase of EBV infection was not enhanced by GFP-dnE1, GFP-dnE1 was able to block the establishment of EBV latency completely during the subacute phase of EBV infection.

Effect of GFP-dnE1 on EBV-encoded latent gene expression. EBV gene expression was tested at 2 days post-infection by quantitative RT-PCR. We focused on the C/Wp activity because it expresses key viral transactivators including EBNA1, -2, -3s, and -LP to boost viral transforming gene expression. We detected C/Wp-driven transcripts in GFP Hi BALL-1 cells as expected. Conversely, C/Wp-driven transcripts were undetectable in GFP-dnE1 Hi and Lo BALL-1 cells, although these cells retained similar EBV DNA levels to GFP-expressing cells (Fig. 4 and Table 3). The Cp-driven transcript was under the limit of detection by RT-PCR, suggesting that the Wp is predominantly activated at the early phase of EBV infection consistent with previous findings.[7] Inhibition of viral gene transcription was not observed in the RNA polymerase III-driven transcript EBER1,[25] and cyclophilin A mRNA levels were similar between GFP- and GFP-dnE1-expressing cells (Fig. 4 and Table 3). This indicates that the effect of GFP-dnE1 on C/Wp activity is specific, and uncovers an active role of EBNA1 in supporting transactiva-

doi: 10.1111/j.1349-7006.2009.01474.x

Table 2. The establishment efficiency of EBV latency

Cell	Emergence of G418-resistant cells†	
BJAB	100%	(6/6)
Daudi	100%	(10/10)
BALL-1		
Parental	56%	(5/9)
GFP Hi	67%	(2/3)
GFP-dnE1 Hi	0%	(0/6)
GFP-dnE1 Lo	0%	(0/6)

†Percentage of wells positive for G418-resistant cells over the number of tested wells from 96-well plates indicated in the bracket. Shown are the sum of two independent experiments. dnE1, dominant-negative EBNA1; EBV, Epstein–Barr virus; GFP, green fluorescent protein.

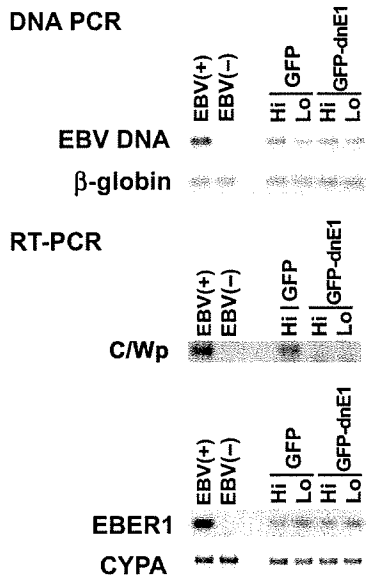

Fig. 4. PCR-based analysis of Epstein–Barr virus (EBV) gene expression. The effect of green fluorescent protein (GFP)-dominant-negative EBNA1 (dnE1) on the loss of EBV DNA (DNA PCR, upper panels) and transcription of the C/W promoter-driven transcript (C/Wp), EBER1, and cyclophilin A (CYPA; RT-PCR, lower panels) in BALL-1 cells at 2 days post-infection were examined. EBV-transformed B-lymphoblastoid cell line (B-LCL) and BJAB cells, denoted as EBV(+) and EBV(−), were used as positive and negative controls for viral DNA and RNA shown, respectively. β-Globin and CYPA were used as controls.

Table 3. Quantification of EBV transcripts in BALL-1 cells by real-time PCR at 2 days post-infection

BALL-1 cells		W1/2 exon (copies†)	EBER1 (copies‡)	CYPA (copies‡)
GFP	Hi	2.2	2.8×10^2	1.4×10^6
	Lo	NT§	0.8×10^2	1.0×10^6
GFP-dnE1	Hi	BLD¶	3.3×10^2	1.3×10^6
	Lo	BLD¶	1.2×10^2	1.5×10^6

†Copies per 13–14 ng total cellular RNA. ‡Copies per 200 ng total cellular RNA. §Not tested. ¶Below the limit of detection. CYPA, cyclophilin A; dnE1, dominant-negative EBNA1; EBV, Epstein–Barr virus; GFP, green fluorescent protein.

tion from C/Wp. Taken together, these results show that inhibition of EBNA1 functions strongly restricts EBV-encoded transforming gene expression and, although there is no detectable effect on the ROL of EBV DNA at the acute phase of viral infection, it blocks the establishment of EBV latency during the subacute phase.

Discussion

This is the first report describing the effect of EBNA1 inhibition from the onset of EBV infection in B cells. Unexpectedly, the dnE1 was unable to accelerate the ROL during the acute phase of EBV infection since dnE1 enhanced the loss of the oriP plasmid in the transient transfection assays.[10,11] In the subacute phase of EBV infection, the establishment of EBV latency was potently blocked by dnE1. In addition, we observed a strong repressive effect of dnE1 on the EBNA1-dependent enhancement of viral gene transcription from C/Wp during the early phase of EBV infection, similar to the transient transfection assays.[17] These data suggest that viral oncogene expression depends heavily on EBNA1 during the acute phase of viral infection, and that EBNA1 contributes little to EBV genome maintenance during this period. The results emphasize that an EBNA1 inhibitor should serve as an attenuator of viral oncogene expression since activation of C/Wp is the 'root' event of the positive feedback loop involved in the transactivation of viral transforming gene expression. In this regard, the EBNA1 inhibition approach could be superior to LMP-1 or EBNA2 inhibition.

If EBNA1 binding to oriP is essential for both the enhancement of viral gene transcription and for genome maintenance, what mechanism prevents dnE1 from affecting the ROL during the acute phase of EBV infection? It is likely that maintenance of the oriP replicon immediately after its introduction into cells is less efficient than in cells harboring an 'established' oriP replicon as an autonomously replicating plasmid. The ROL of an established oriP replicon is 2–4% per cell generation.[10,11] In contrast, our data from the EBV/B cell-based assay gave an average ROL of 26–38% during the week post-infection (acute phase of EBV infection). In agreement with our findings, it is reported that a transiently transduced oriP replicon is lost from cells at 26–37% per cell generation 1–2 weeks post-plasmid transduction.[12] These data indicate that maintenance of the oriP replicon is largely EBNA1-independent immediately after its introduction into cells, regardless of whether the route of introduction is by transfection or EBV infection. In other words, the establishment of EBV latency should be a rare epigenetic event. The data also suggest that the artificial minichromosome approach may be relevant in understanding EBV genome behavior.[12]

Our study suggests that gene therapy using GFP-dnE1 is an attractive approach, not only for therapeutics, but also for prophylactic interventions of EBV-associated malignancies. For example, in peripheral blood stem cell transplantation (PBSCT), GFP-dnE1 transduction into $CD34^+$ cells should protect the differentiated B cells from EBV infection, thus preventing the genesis of EBV-associated B cell lymphomas. We will attempt to prove this hypothesis using a small animal model in future studies.[26] Additionally, EBNA1 is a potential molecular target for developing a small molecular-weight EBV inhibitor as mentioned previously.[14,15] The advantages of EBNA1-inhibitor development are that the biological assay system is already established and the X-ray crystal structure of the DNA-bound EBNA1 DNA binding and dimerization domain is known, which means that computer-aided drug design technology can be immediately applied. Although EBV is associated with various malignancies, preventive and therapeutic measures against EBV infection have not been developed. We believe that an anti-EBV agent, such as an EBNA1 inhibitor, would have an enormous impact in the medical field due to the substantial number of patients with EBV-associated malignancies.

Acknowledgments

We thank Drs Kenichi Imadome and Shigeyoshi Fujiwara for reagents. We also thank Dr Bill Sugden for critically reading the manuscript. This work was supported by the Japan Health Science Foundation, the Ministry of Health, Labor and Welfare of Japan, and the Ministry of Education, Culture, Sports, Science and Technology of Japan.

Disclosure Statement

The authors have no conflict of interest.

References

1 Thompson MP, Kurzrock R. Epstein–Barr virus and cancer. *Clin Cancer Res* 2004; **10**: 803–21.
2 Rickinson AB, Kieff E. Epstin–Barr virus. In: Knipe DM, Howley PM, eds. *Fields Virology*, 5th edn, vol. 2. Philadelphia: Lippincott Williams & Wilkins, 2007; 2655–700.
3 Klein E, Kis LL, Klein G. Epstein–Barr virus infection in humans: from harmless to life endangering virus-lymphocyte interactions. *Oncogene* 2007; **26**: 1297–305.
4 Snow AL, Martinez OM. Epstein–Barr virus: evasive maneuvers in the development of PTLD. *Am J Transplant* 2007; **7**: 271–7.
5 Besson C, Goubar A, Gabarre J *et al.* Changes in AIDS-related lymphoma since the era of highly active antiretroviral therapy. *Blood* 2001; **98**: 2339–44.
6 Carbone A, Cesarman E, Spina M, Gloghini A, Schulz TF. HIV-associated lymphomas and gamma-herpesviruses. *Blood* 2009; **113**: 1213–24.
7 Kieff E, Rickinson AB. Epstin–Barr virus and its replication. In: Knipe DM, Howley PM, eds. *Fields Virology*, 5th edn, vol. 2. Philadelphia: Lippincott Williams & Wilkins, 2007; 2603–54.
8 Lindner SE, Sugden B. The plasmid replicon of Epstein–Barr virus: mechanistic insights into efficient, licensed, extrachromosomal replication in human cells. *Plasmid* 2007; **58**: 1–12.
9 Wang J, Sugden B. Origins of bidirectional replication of Epstein–Barr virus: models for understanding mammalian origins of DNA synthesis. *J Cell Biochem* 2005; **94**: 247–56.
10 Kirchmaier AL, Sugden B. Plasmid maintenance of derivatives of oriP of Epstein–Barr virus. *J Virol* 1995; **69**: 1280–3.
11 Sugden B, Warren N. Plasmid origin of replication of Epstein–Barr virus, oriP, does not limit replication in cis. *Mol Biol Med* 1988; **5**: 85–94.
12 Leight ER, Sugden B. Establishment of an oriP replicon is dependent upon an infrequent, epigenetic event. *Mol Cell Biol* 2001; **21**: 4149–61.
13 Hurley EA, Thorley-Lawson DA. B cell activation and the establishment of Epstein–Barr virus latency. *J Exp Med* 1988; **168**: 2059–75.
14 Altmann M, Pich D, Ruiss R, Wang J, Sugden B, Hammerschmidt W. Transcriptional activation by EBV nuclear antigen 1 is essential for the expression of EBV's transforming genes. *Proc Natl Acad Sci U S A* 2006; **103**: 14188–93.
15 Kennedy G, Komano J, Sugden B. Epstein–Barr virus provides a survival factor to Burkitt's lymphomas. *Proc Natl Acad Sci U S A* 2003; **100**: 14269–74.
16 Nasimuzzaman M, Kuroda M, Dohno S *et al.* Eradication of Epstein–Barr virus episome and associated inhibition of infected tumor cell growth by adenovirus vector-mediated transduction of dominant-negative EBNA1. *Mol Ther* 2005; **11**: 578–90.
17 Kirchmaier AL, Sugden B. Dominant-negative inhibitors of EBNA-1 of Epstein–Barr virus. *J Virol* 1997; **71**: 1766–75.
18 Komano J, Miyauchi K, Matsuda Z, Yamamoto N. Inhibiting the Arp2/3 complex limits infection of both intracellular mature vaccinia virus and primate lentiviruses. *Mol Biol Cell* 2004; **15**: 5197–207.
19 Aiyar A, Sugden B. Fusions between Epstein–Barr viral nuclear antigen-1 of Epstein–Barr virus and the large T-antigen of simian virus 40 replicate their cognate origins. *J Biol Chem* 1998; **273**: 33073–81.
20 Middleton T, Sugden B. EBNA1 can link the enhancer element to the initiator element of the Epstein–Barr virus plasmid origin of DNA replication. *J Virol* 1992; **66**: 489–95.
21 Urano E, Kariya Y, Futahashi Y *et al.* Identification of the P-TEFb complex-interacting domain of Brd4 as an inhibitor of HIV-1 replication by functional cDNA library screening in MT-4 cells. *FEBS Lett* 2008; **582**: 4053–8.
22 Shimizu S, Urano E, Futahashi Y *et al.* Inhibiting lentiviral replication by HEXIM1, a cellular negative regulator of the CDK9/cyclin T complex. *AIDS* 2007; **21**: 575–82.
23 Kanda T, Yajima M, Ahsan N, Tanaka M, Takada K. Production of high-titer Epstein–Barr virus recombinants derived from Akata cells by using a bacterial artificial chromosome system. *J Virol* 2004; **78**: 7004–15.
24 Mackey D, Sugden B. The linking regions of EBNA1 are essential for its support of replication and transcription. *Mol Cell Biol* 1999; **19**: 3349–59.
25 Howe JG, Shu MD. Epstein–Barr virus small RNA (EBER) genes: unique transcription units that combine RNA polymerase II and III promoter elements. *Cell* 1989; **57**: 825–34.
26 Yajima M, Imadome K, Nakagawa A *et al.* A new humanized mouse model of Epstein–Barr virus infection that reproduces persistent infection, lymphoproliferative disorder, and cell-mediated and humoral immune responses. *J Infect Dis* 2008; **198**: 673–82.

doi: 10.1111/j.1349-7006.2009.01474.x

Targeted Delivery of Immunogen to Primate M Cells with Tetragalloyl Lysine Dendrimer[1]

Shogo Misumi,[2]* Mitsuaki Masuyama,[2]*† Nobutoki Takamune,* Daisuke Nakayama,* Ryotarou Mitsumata,* Hirokazu Matsumoto,* Norimitsu Urata,* Yoshihiro Takahashi,† Atsunobu Muneoka,† Takayuki Sukamoto,† Koichiro Fukuzaki,† and Shozo Shoji[3]*‡

Effective uptake of Ags by specialized M cells of gut-associated lymphoid tissues is an important step in inducing efficient immune responses after oral vaccination. Although stable nontoxic small molecule mimetics of lectins, such as synthetic multivalent polygalloyl derivatives, may have potential in murine M cell targeting, it remains unclear whether synthetic multivalent polygalloyl derivatives effectively target nonhuman and human M cells. In this study, we evaluated the ability of a tetragalloyl derivative, the tetragalloyl-D-lysine dendrimer (TGDK), to target M cells in both in vivo nonhuman primate and in vitro human M-like cell culture models. TGDK was efficiently transported from the lumen of the intestinal tract into rhesus Peyer's patches by M cells and then accumulated in germinal centers. Oral administration of rhesus CCR5-derived cyclopeptide conjugated with TGDK in rhesus macaque resulted in a statistically significant increase in stool IgA response against rhesus CCR5-derived cyclopeptide and induced a neutralizing activity against SIV infection. Furthermore, TGDK was specifically bound to human M-like cells and efficiently transcytosed from the apical side to the basolateral side in the M-like cell model. Thus, the TGDK-mediated vaccine delivery system represents a potential approach for enabling M cell-targeted mucosal vaccines in primates. ***The Journal of Immunology,*** **2009, 182: 6061–6070.**

Human immunodeficiency virus is transmitted primarily via the genital mucosa during sexual intercourse. Elucidating the early events in mucosally transmitted HIV-1 infection plays a critical role in characterizing the virus-host interactions and effective vaccine design and development. Mucosal transmission of HIV-1 infection is mediated by exposure to cell-free viruses and/or cell-associated viruses within mucosal secretions, and established within hours, and can be disseminated to draining lymph nodes within days (1, 2). Recent studies of pathological events in acute infection in nonhuman primates and humans have provided important insights into the disruption of the mucosal immune system. This disruption is evident in the rapid depletion of $CD4^+$ T cells within the GALT during acute infection (3, 4), suggesting that once mucosal infection has occurred, immune responses to infection are insufficient to prevent these events. Therefore, a preventive vaccine should effectively target the earliest events in the establishment of HIV infection at the mucosal site.

Conventional vaccines administered from any routes other than the oral route effectively induce protective systemic immune responses, but the level of protective immunity at the major site of HIV mucosal entry is less robust. However, neutralizing Abs administered i.v. at high doses can reach mucosal sites and block genital mucosal transmission of simian/HIV (SHIV)[4] in nonhuman primate models (5), suggesting that sufficient mucosal humoral immune responses induced by mucosal vaccines can prevent HIV infection. Some related studies have shown that mucosal vaccines induce not only secretory IgA at mucosal sites, but also mucosal cell-mediated immunity and systemic Abs against HIV (6–13). These studies suggest that mucosal vaccines have several advantages over conventional systemic vaccines because they can induce multi-immuno responses that prevent HIV infection at the mucosal site.

Current efforts to develop effective mucosal vaccines are mainly directed toward finding more efficient means of delivering appropriate Ags to the mucosal immune system and toward developing effective and safe mucosal adjuvants (14) because it has often proved difficult to stimulate strong mucosal IgA immune responses and protection against pathogens by mucosal administration of Ags without Ag delivery and adjuvant systems. It is generally accepted that M cells in Peyer's patches (PPs) are instrumental in initiating mucosal immunity against pathogens invading across epithelial barriers (15). The high transcytotic abilities of M cells

*Department of Pharmaceutical Biochemistry, Faculty of Medical and Pharmaceutical Sciences, Kumamoto University, Kumamoto, Japan; †Shin Nippon Biomedical Laboratories, Kagoshima, Japan; and ‡Kumamoto Health Science University, Kumamoto, Japan

Received for publication September 3, 2008. Accepted for publication March 13, 2009.

The costs of publication of this article were defrayed in part by the payment of page charges. This article must therefore be hereby marked *advertisement* in accordance with 18 U.S.C. Section 1734 solely to indicate this fact.

[1] This study was supported in part by a Grant-in-Aid for scientific research from the Ministry of Education, Culture, Sports, Science, and Technology of Japan, and a health science research grant from the Ministry of Health, Labor, and Welfare of Japan.

[2] S.M. and M.M. contributed equally to this work.

[3] Address correspondence and reprint requests to Dr. Shozo Shoji, Kumamoto University, Department of Pharmaceutical Biochemistry, Faculty of Medical and Pharmaceutical Sciences, 5-1 Oe-Honmachi, Kumamoto 862-0973, Japan. E-mail address: shoji@gpo.kumamoto-u.ac.jp

www.jimmunol.org/cgi/doi/10.4049/jimmunol.0802928

[4] Abbreviations used in this paper: SHIV, simian/HIV; DAPI, 4′,6-diamidino-2 phenylindole; DIC, differential interference contrast; DMF, dimethylformamide; EDS, energy-dispersive x-ray spectroscopy; FAE, follicle-associated epithelium; Fmoc, 9-fuorenylmethoxycarbonyl; GC, germinal center; PEG, polyethylene glycol; PP, Peyer's patch; PV, poliovirus; rcDDR5, rhesus CCR5-derived cyclopeptide; RT, room temperature; SMPD, synthetic multivalent polygalloyl derivative; TEM, transmission electron microscopy; TGDK, tetragalloyl-D-lysine dendrimer; TRITC, tetramethylrhodamine isothiocyanate; UEA-1, *Ulex europaeus agglutinin-1*; wpim, weeks postinitial immunization.

make them an attractive target for mucosally delivered vaccines because mucus secretion may flush away an applied mucosal vaccine at the mucosal site. Some studies showed that mucosal vaccine delivery can be improved using appropriate bioadhesin molecules such as lectins because M cell surface glycocalyx differs in carbohydrate composition from that of enterocytes in many species (16–22). *Ulex europaeus agglutinin-1* (UEA-1)-conjugated (23, 24) or σ1 protein-conjugated nasal vaccination (13, 25) induces not only strong Ag-specific mucosal IgA and plasma IgG responses, but also CTL immunity. However, lectins such as UEA-1 are of limited value in vaccine delivery because they are toxic and subject to intestinal degradation. Lambkin et al. (26) reported that a stable low m.w. four-copy gallic acid construct is a competitor of UEA-1 and appears to have high affinity for the fucose receptor on murine M cells. Although stable nontoxic small molecular mimetics of UEA-1 have the potential for M cell targeting in mice, it remains unclear whether these mimetics effectively target the nonhuman and human M cells.

In this study, we synthesized the tetragalloyl-D-lysine dendrimer (TGDK) and demonstrated its M cell targeting potential in both in vivo nonhuman primate and in vitro human M-like cell culture models.

Materials and Methods

TGDK and D-lysine dendrimer

The 9-fuorenylmethoxycarbonyl (Fmoc)-D-MAP_4-NH-(CH_2)-NH-Trt-resin (in this study referred to as Fmoc-D-lysine dendrimer resin; Watanabe Chemical Industries) was treated with 20% piperidine/dimethylformamide (DMF) for 20 min to remove the Fmoc group. To prepare TGDK, the resin (0.51 mmol) was then washed five times with DMF and reacted with 3,4,5-trimethoxybenzoic acid chloride (1 mmol) in triethylamine (7 mmol) at 40°C for 120 min. The resulting resin was washed with 1% triethylamine/DMF three times and DMF five times, and then treated with boron tribromide (the amount is 20× mole equivalent of that of DMF in the reaction mixture) at 40°C for 5 min before air drying. TGDK was extracted with Milli-Q water, purified, and lyophilized. The patent for the synthesis method of TGDK has been obtained (PCT/JP2006/321720). The D-lysine dendrimer was obtained by treating the D-lysine dendrimer resin with acetic acid/trifluoroethanol/dichloromethane (1:1:8). The molecular masses of TGDK and D-lysine dendrimer were determined by MALDI-TOF mass spectrometry (Burker Franzen Analytik).

Animals and tissue samples

Purpose-bred female rhesus macaques (*Macaca mulatta*) obtained from a supplier in China (4–6 years old) were used for this study. This study (permission no. 19-137) was approved and conducted in accordance with the guidelines of the Animal Care and Use Committee of Kumamoto University.

Inoculation of TGDK

Rhesus macaques were fasted overnight. They were then inoculated with 1 ml of FITC-labeled TGDK solution (100 nmol) or 0.5 ml of 10 nm gold-labeled TGDK at a site in the ileum (15 cm from the cecum) after celiotomy under anesthesia induced by a s.c. injection of urethane (ethyl carbamate, 800 mg/ml; 1.5 ml/kg body weight; Wako Pure Chemical) solution and an i.v. injection of α-chloralose (Wako Pure Chemical; 20 mg/ml; 5.5 ml/kg body weight) into the cephalic vein.

Inoculation of poliovirus (PV)

Rhesus macaques were fasted overnight. They were then inoculated with PV solution at a site in the ileum (15 cm from the cecum), as described previously (27).

Collection of PPs

The rhesus monkeys were euthanized by exsanguination under anesthesia, and the part of the ileum (15 cm from cecum) including the inoculation site was collected. After washing the collected part of the ileum, the blocks of PPs were embedded in the OCT compound (Sakura Finetechnical) for immunofluorescence staining or fixed in ice-cold 3% glutaraldehyde/0.1 M sucrose/PBS (pH 7.4) for transmission electron microscopy and energy-dispersive x-ray spectroscopy.

Histopathological study

Tissue samples were fixed in 10% neutral buffered formalin and were trimmed, embedded in paraffin, sectioned, stained with H&E, and examined by light microscopy.

Immunofluorescence staining

To examine the binding and tissue localizations of TGDK, 5 μm frozen sections derived from rhesus macaques inoculated with FITC-labeled TGDK solution were fixed in cold acetone and blocked with 1% nonfat skim milk in PBS^-. FITC-labeled TGDK was detected using a rabbit anti-FITC Ab (Zymed Laboratories) for signal amplification and a tetramethylrhodamine isothiocyanate (TRITC)-labeled anti-rabbit IgG Ab or an Alexa488-labeled anti-rabbit IgG Ab as a secondary Ab. To further examine how TGDK is incorporated into the lymphoid organ, the sections were stained with a PE-labeled anti-CD20 Ab (BD Biosciences) or an anti-CD54 Ab (R&D Systems) labeled with Alexa555 using a Zenon mouse IgG labeling kit (Invitrogen).

To investigate whether gp2 was expressed in rhesus PP M cells, the sections were pretreated with 0.1% Triton X-100, which is used to solubilize the mucus, and then stained with an anti-PV Ab (II-MAP-01; Japan Poliomyelitis Research Institute) labeled with Alexa488 using a Zenon mouse IgG labeling kit (Invitrogen Corporation) or a rabbit anti-gp2 Ab (IMGENEX) labeled with Alexa555 using a Zenon rabbit IgG labeling kit (Invitrogen). To further examine how FITC-labeled TGDK specifically binds to PP M cells, the sections were also pretreated with 0.1% Triton X-100 and then stained with a rabbit anti-FITC Ab and Alexa488-labeled anti-rabbit IgG Ab as a secondary Ab or a rabbit anti-gp2 Ab (IMGENEX) labeled with Alexa555 using a Zenon rabbit IgG labeling kit (Invitrogen). Some sections were counterstained with 4′,6-diamidino-2 phenylindole (DAPI) to show nuclei.

After the staining, slides were washed and analyzed with a Keyence Biozero BZ-8000 (Keyence) and a Flowview FV3000 (Olympus).

Transmission electron microscopy (TEM) and energy-dispersive x-ray spectroscopy (EDS)

Tissue samples were rinsed in PBS with 0.1 M sucrose (pH 7.4) and post-fixed with 1% osmium tetroxide in 0.1 M phosphate buffer at 4°C for 2 h. All the samples were rinsed briefly with 50:50, 70:30, 80:20, 90:10, and 95:5 ethanol/water mixtures and 100% ethanol for 10 min each and three times with 100% ethanol for dehydration, and then embedded in epoxy resin (Quatol 812). One-micrometer sections were cut using a glass knife and then stained with toluidine blue. Suitable areas for ultrastructural study were chosen after examining 1-μm sections under a light microscope. Sections of 60–90 nm were cut on a Leica EM UC6 ultramicrotome using a diamond knife, and sections were mounted on a copper grid and stained with 1% uranyl acetate and Reynolds lead citrate. The grids were examined under a JEOL JEM 1200-EX electron microscope. Furthermore, EDS, which was consigned to JEOL Datum, was performed to quantify TGDK by measuring gold concentration within a specimen.

Preparation of TGDK-conjugated multiantigens

To examine the in vivo effect of TGDK on M cell targeting, TGDK was conjugated via a Hubantigen with rhesus CCR5-derived cyclopeptide (rcDDR5) and BSA. To prepare a Hubantigen, an eight-arm functional polyethylene glycol (PEG) with *p*-nitrophenyl groups, SUNBRIGHT HGEO-200NP (NOF Corporation; 1 equivalent), was mixed with an eight-arm functional PEG with primary amino groups, SUNBRIGHT HGEO-200PA (NOF; 7.2 equivalent), in DMF for 16 h. The resulting Hubantigen was dialyzed in Spectrapore dialysis bags (Spectrum Laboratories; molecular weight cut off = 12–14 kDa) against Milli-Q water for 2 days. The dialysate was lyophilized and used as a Hubantigen. To prepare rcDDR5, a rhesus CCR5-derived linear dodecapeptide (H_2N-KRSQREGLHYTG-COOH), in which all side-chain groups are protected, was synthesized using an automatic peptide synthesizer, and cyclized, as previously described (28). To bind both TGDK and rcDDR5 to the Hubantigen, the amino group of ethylenediamine in TGDK (two equivalents) or of Lys^1 in the deprotected rcDDR5 (two equivalents) was conjugated to four-armed functional PEG, SUNBRIGHT PTE-100NP (NOF; 1 equivalent). Finally, the Hubantigen (168 mg) was coupled to the four-armed PEG-ylated TGDK (12 μmol) and -rcDDR5 (12 μmol) in DMF for 24 h and then covalently bound to BSA for 6 h. The TGDK-conjugated Ag was dialyzed for 15 h against PBS^-, and the dialysate was lyophilized with lactose. The resulting Ag was encapsulated in enteric-coated capsules and included TGDK (56 nmol/capsule), rcDDR5 (90 nmol/capsule), lactose (146 μmol/capsule), and BSA (4.5 nmol/capsule). In contrast, a control Ag also included BSA (4.5 nmol/capsule), but it was not conjugated via a covalent

bond with a Hubantigen. Furthermore, the control Ag did not include TGDK and rcDDR5.

Immunization schedule

All of the rhesus macaques were housed in individual cages and maintained in accordance with the rules and guidelines of the National Institute for Infectious Diseases for experimental animal welfare. Five 4- to 6-year-old rhesus macaques (no. 6–10) were orally administered with two enteric-coated capsules containing TGDK-conjugated multiantigens at 0, 2, and 6 wk. Another five rhesus macaques (no. 1–5) were immunized with an enteric-coated capsule including control Ag following the same immunization schedule as that for the controls. Stool samples were obtained at 0, 12, 13, and 14 wk postinitial immunization (wpim), which were then subjected to anti-BSA Ab ELISA and rcDDR5-coupled multipin ELISA in accordance with the method of Misumi et al. (29).

Sample collection and processing

Acetone powder was prepared by adding fecal pellets (3 g) with stirring to 3 ml of cold acetone. The powder was then washed three times with cold ether and dried until no trace of ether remained. The acetone powder (100 mg) was resuspended in 400 μl of 1% MPC polymer solution (NOF) and incubated at 37°C for 30 min, and then on ice for 1 h. The suspensions were centrifuged at 13,000 × *g* for 5 min to remove fecal solids. The processed fecal Ab samples were subjected to anti-BSA Ab ELISA and rcDDR5-coupled multipin ELISA.

Anti-BSA Ab ELISA

Abs against BSA in stool samples were detected by ELISA. For evaluation of stool Abs, each well of a flat-bottom 96-well maxisorp microplate (Nunc) was coated with 50 μl of coating buffer (pH 8.0) containing BSA (100 μg/ml) and incubated at room temperature (RT) overnight. The wells were washed with 150 μl of Milli-Q water with 0.1% Tween 80 with complete decanting and rinsed with Milli-Q water. Subsequently, 100 μl of blocking buffer, composed of 1% skim milk in Milli-Q water, was added to each well and incubated for 2 h at RT to occupy all unbound sites. Washing was repeated, as described above, followed by the addition of 50 μl of a fecal Ab sample diluted 1/10 in PBS^- to each well. Plates were incubated for 2 h at RT and then washed with 0.1% Tween 80, and 50 μl of peroxidase-conjugated goat anti-monkey IgA (diluted 1/5000) was added to each well and incubated for 1 h at RT before the plate was washed. Fifty microliters 3,3′,5,5′-tetramethylbenzidine solution (Wako Pure Chemical) as the substrate was added to each well and incubated at room temperature. Absorbance was measured at 450/630 nm using a microplate reader.

rcDDR5-coupled multipin ELISA

A rhesus CCR5-derived linear dodecapeptide (H_2N-ERSQREGLHYTG-COOH) in which all side-chain groups are protected was synthesized using an automatic peptide synthesizer and was cyclized by bond formation between the α-carboxyl group of Gly and the α-amino group of Glu after removal of the resin. The γ-carboxyl group of Glu in the protected cyclic dodecapeptide was conjugated to MultiPin block (Mimotopes). The block was used for detecting anti-CCR5 Abs in stool samples in accordance with the method of Misumi et al. (28).

Determination of total number of SIV DNA copies

The total number of SIVmac239 DNA copies was determined to monitor SIV infection and estimate the neutralizing activity of antisera. The relative change in the number of SIV DNA copies indicates the degree of neutralizing activity. Percentage of copies in HSC-F infected with SIVmac239 in the presence of a 14-wpim stool sample is expressed relative to that in the presence of a 0-wpim stool sample, which is considered 100%. HSC-F cells (4×10^6) were infected with SIVmac239 (50 ng, measured using p27 Ag) in the presence of the 0- and 14-wpim stool samples, dialyzed (cutoff, 100 kDa) against PBS^-, and diluted in PBS^-. The inhibitory effect of the stool sample was investigated at 55-fold final dilution. After 48 h, HSC-F cells were harvested. The total viral DNA obtained after the purification procedure (29) was used for SYBR Green real-time PCR assay, as previously described (30), with some modifications. Briefly, primers that recognize specific and highly conserved sequences on the *gag* region of SIV described by Ui et al. (31) were selected. The sequences of SIV *gag* primers were 5′-GGAAATTACCCAGTACAACAAATAGG-3′ and 5′-TC TATCAATTTTACCCAGGCATTTA-3′. The SIV *gag* gene was amplified in 20 μl of a PCR mixture consisting of 10 μl of 2× master mix containing modified DyNAmo hot start DNA polymerase, SYBR Green I, optimized PCR buffer, 5 mM $MgCl_2$, a dNTP mix including dUTP (Finnzymes), 2 μl of each primer, and 8 μl of cDNA. PCR was conducted as follows: initial activation of hot start DNA polymerase at 95°C for 15 min; 40 cycles of four steps of 95°C for 10 s, 57°C for 20 s, 72°C for 20 s, and 76°C for 2 s. At the end of the amplification cycle, melting temperature analysis was conducted by gradually increasing temperature (0.5°C/s) to 95°C. Amplification, data acquisition, and analysis were conducted with the DNA Engine Opticon 2 System (Bio-Rad) using Opticon Monitor version 3.0 software.

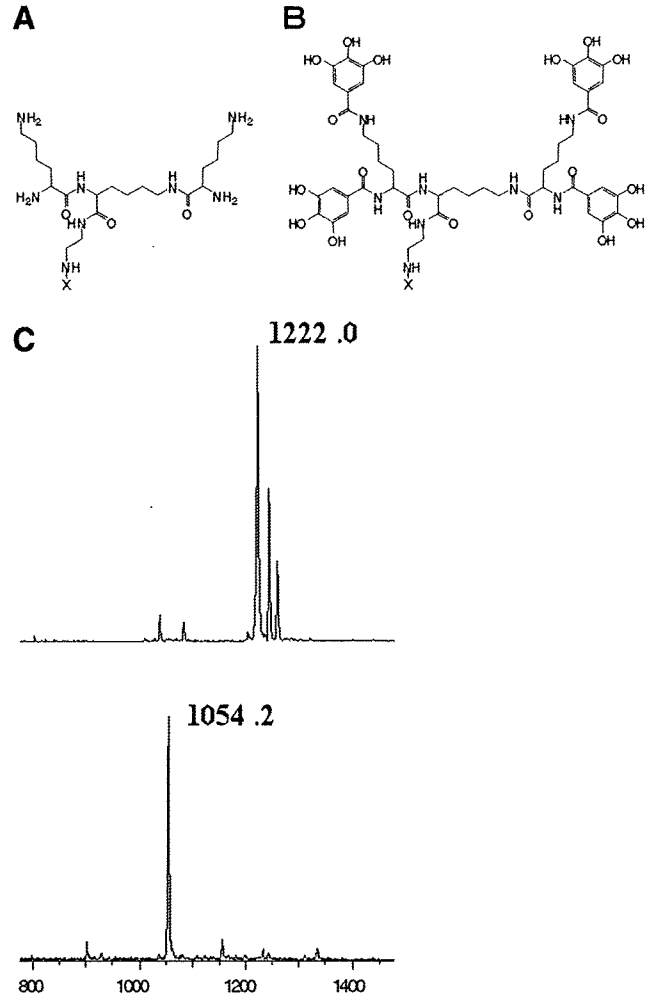

FIGURE 1. Structure and mass spectrometry of TGDK. *A*, D-lysine dendrimer. *B*, TGDK. *C*, MALDI-TOF mass spectrometry spectrum of intermediate compound, $(3,4,5\text{-trimethoxybenzoyl})_4$-D-lyseine dendrimer, and TGDK. The spectra exhibited two peaks at m/z 1222.0 and 1054.2: the *upper peak* is that of the ion derived from the reaction intermediate, $(3,4,5\text{-trimethoxybenzoyl})_4$-D-lyseine dendrimer, and the *lower peak* is that of the ion derived from TGDK.

In vitro human M cell model

The human M cell model was constructed using cocultures of Caco-2 cells and Raji cells in accordance with the method of Kernéis et al. (32) with slight modification. We seeded Caco-2 cells by adding 1×10^6 cells on the lower face of 3-μm-pore Transwell filters and culturing them overnight. The filters were then transferred to the Transwell device with the epithelial cells facing the lower chamber of the cluster plates. Caco-2 cells were cultured until they were fully differentiated (21 days). Raji B cells (10^6) were added to the upper chamber facing the basolateral side of Caco-2 cells. The cultures were maintained for 3 days. Caco-2 cell monolayers were washed with PBS^- and incubated with FITC-labeled TGDK, or FITC-labeled D-lysine dendrimer with or without PV (type II, $10^{4.5}$–$10^{5.5}$ cell culture infective doses 50%) for 30 min. To examine the localization of PV and M cell makers (i.e., gp2, CD54, and integrin β_1), the monolayers were stained with an anti-PV Ab (II-MAP-01; Japan Poliomyelitis Research Institute), an anti-gp2 polyclonal Ab (IMGENEX) labeled with

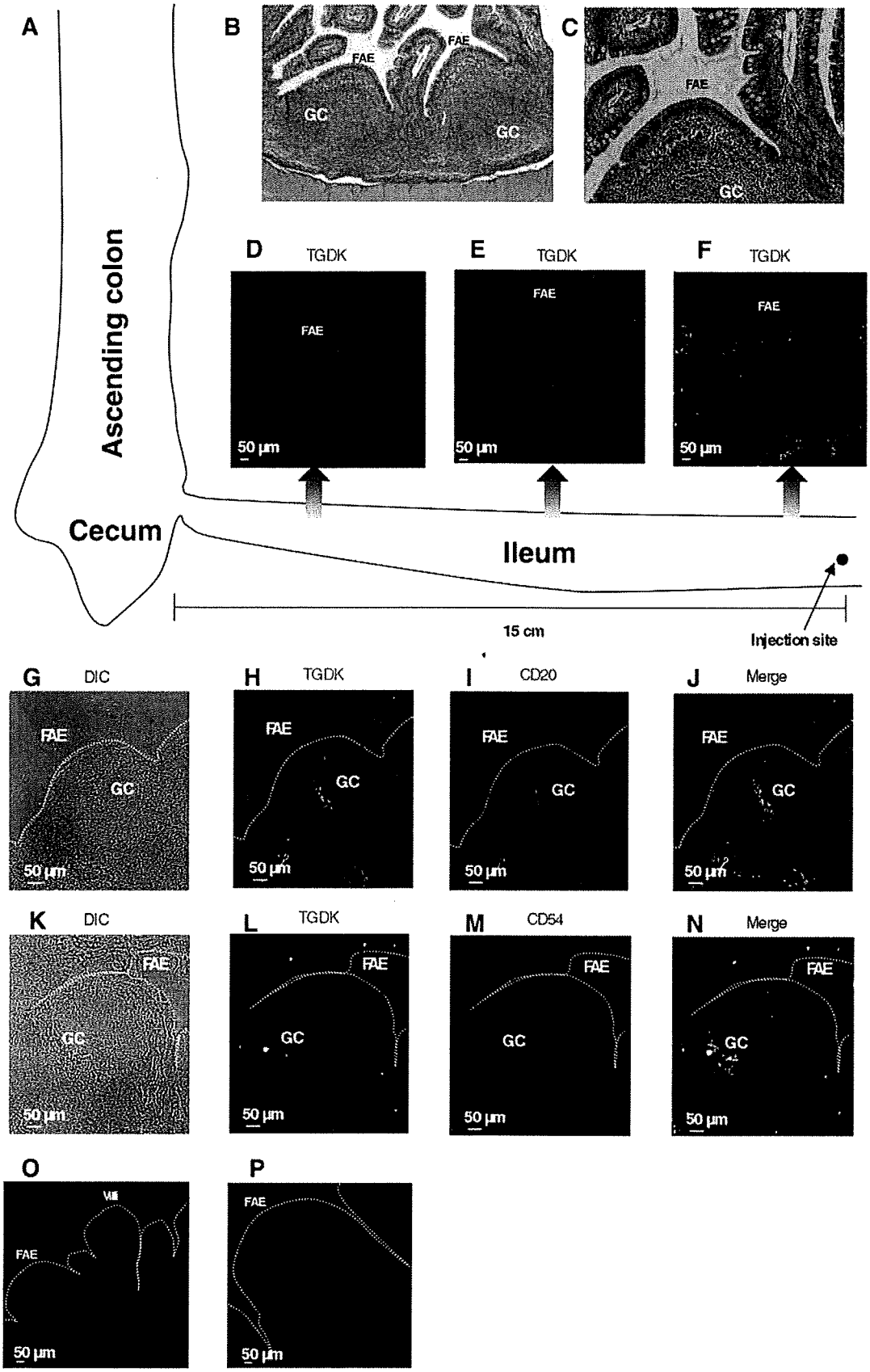

FIGURE 2. Association of TGDK with rhesus PP FAE and accumulation of TGDK within the GCs. *A*, Schematic diagram of rhesus ileum. *B* and *C*, H&E staining of rhesus PPs. *D–F*, FITC-labeled TGDK was inoculated into the lumen of the ileum at 15 cm from the ileocecal valve. One hour after TGDK inoculation, the portion between the injection site of TGDK and the ileocecal valve was excised and subjected to immunofluorescence analysis. Frozen sections of rhesus macaque PPs were labeled with mAbs (anti-CD20 Ab (*I*) and anti-CD54 Ab (*M*); red), and TGDK was stained, as described in *Materials and Methods* (red or green) (*D–F*, *H*, and *L*). Differential interference contrast (DIC) (*G* and *K*), merged (*J* and *N*), and control (*O*, Alexa488-labeled anti-rabbit IgG, or *P*, TRITC-labeled anti-rabbit IgG) images are shown.

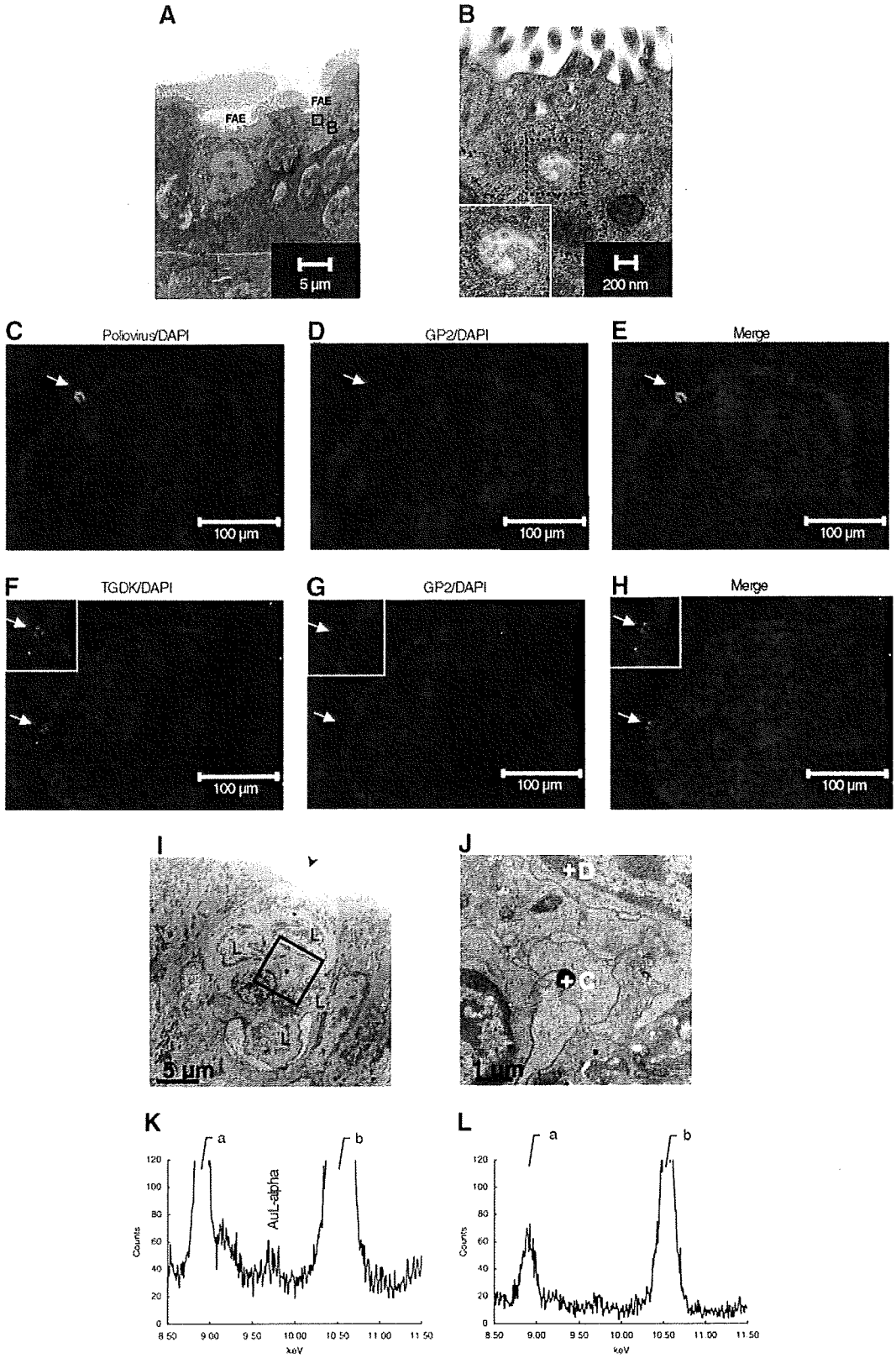

FIGURE 3. TGDK can efficiently penetrate into rhesus PP M cells. PV, FITC-labeled TGDK, or 10-nm gold-labeled TGDK was inoculated into the lumen of the ileum, as described in *Materials and Methods*. After the inoculation, the portion between the inoculation site and the ileocecal valve was excised and subjected to electron microscopies (*A*, *B*, *I*, and *J*), immunofluorescence analysis (*C–H*), or EDS (*K* and *L*). *A*, TEM image of typical M cells in the PP. *B*, TEM image of *B* shown in *A*. *Inset* (the magnified TEM image of dotted square in *B*), PV is transcytosed through rhesus PP M cells. *C–H*, Frozen sections of rhesus macaque PPs were labeled with mAbs (anti-PV Ab (*C*) and anti-gp2 Ab (*D* and *G*)), and TGDK were stained, as described in *Materials and Methods* (*F*). Merged images are shown (*E* and *H*). *I*, TEM view of rhesus PP M cells, which had short (arrowhead) and irregular microvilli and pocket structures containing lymphocytes (indicated by *L*). *J*, Depicts a higher-magnification image of *I*. *K* and *L*, Graphs show EDS of *spots C* and *D* in *J*, confirming the presence of gold-labeled TGDK. The *a* signals come from Cu (8.904 keV), which is attributed to the sample holder, and the *b* signal contains the signal of OsLβ (10.354 keV).

Alexa555 using a Zenon mouse IgG labeling kit (Invitrogen), a mouse anti-human CD54 Ab (R&D Systems), or a mouse anti-human integrin $\alpha_5\beta_1$ Ab (Chemicon International), and then incubated with or without TRITC-labeled goat anti-mouse IgG (Jackson ImmunoResearch Laboratories). At the end of the staining, slides were washed and incubated with DAPI for nuclear staining. Finally, the monolayers were washed and analyzed with a Keyence Biozero BZ-8000. To investigate whether TGDK was specifically transported in human M cell model, the assay was conducted in the presence of 100 μM FITC-labeled TGDK or FITC placed in the lower chamber. The monolayers including M cells or Caco-2 control monolayers were incubated for 2 h at 37°C. FITC-labeled TGDK or FITC, transported from the lower chamber to the upper chamber, was quantified using a CORONA Multi Microplate Reader.

Results

Synthesis of TGDK

UEA-1, an α-L-fucose-specific lectin, has been of particular interest owing to its M cell specificity in the mouse model and its applicability to proof-of-concept studies of vaccine delivery to APCs (33). However, lectins are susceptible to proteolytic degradation in the gastrointestinal tract, and their cytotoxic effects also limit their use as targeting agents to deliver vaccines to M cells. One approach to overcoming these limitations is to synthesize small organic molecules that are able to mimic the function of lectins. Lambkin et al. (26, 34) reported that a synthetic multivalent polygalloyl derivative (SMPD) is a competitor of UEA-1 and appears to have high affinity for the fucose receptor on murine M cells. Its advantages include its stability and suitability for incorporation into delivery systems using routine chemical procedures. In this study, we also chose a versatile scaffold with branched D-lysine (Fig. 1*A*). An aminoethyl group was introduced into the lysine dendrimeric scaffold to allow its linkage with a candidate immunogen. Furthermore, gallic acid was selected as a polyphenolic functional group and coupled with α- and ε-amino groups of lysine residues in the lysine dendrimer (Fig. 1*B*). As shown in Fig. 1*C*, the spectra of purified $(3,4,5\text{-trimethoxybenzoyl})_4$-D-lysine dendrimer and TGDK exhibited major peaks at m/z 1222.0 (Fig. 1*C*, *upper spectrum*) and 1054.2 (Fig. 1*C*, *lower spectrum*), respectively. The difference in molecular mass indicates the complete deprotection of the methyl group by boron tribromide.

TGDK transport through follicle-associated epithelium (FAE) of rhesus macaque PPs

To examine whether TGDK was effectively transported through FAE of PPs in vivo, FITC-labeled TGDK was inoculated into the rhesus macaque ileum (Fig. 2*A*). One hour after the injection, the tissue was subjected to immunofluorescence analysis. As shown in Fig. 2, *B* and *C*, the large PP is found in the lumen of the terminal ileum in rhesus macaques. Light microscopy revealed the typical structure of a mucosal lymphoid follicle, composed of germinal centers (GCs) and a dome area bulging into the lumen (Fig. 2, *B* and *C*). The closer the section to the injection site, the larger the amount of TGDK reaching GCs through FAE of PPs (Fig. 2, *D–F*). When PPs from different sections (~7.5 cm from the injection site) were further observed, TGDK was clearly detected in the GCs of PPs (Fig. 2, *H* and *L*). GC cells can be stained with anti-CD20 and anti-CD54 Abs, the staining patterns reflecting reactivity with B cell lymphocytes and the follicular dendritic reticulum in nonhuman primates and humans, respectively (35–37). As shown in Fig. 2, *I* and *M*, CD20 and CD54 were expressed within the GCs of rhesus macaques. Fig. 2, *J* and *N*, shows the patterns of double fluorostaining for TGDK/CD20 or TGDK/CD54 in the GCs of PPs. These results indicate that TGDK efficiently enters into GCs through FAE of PPs in rhesus macaques.

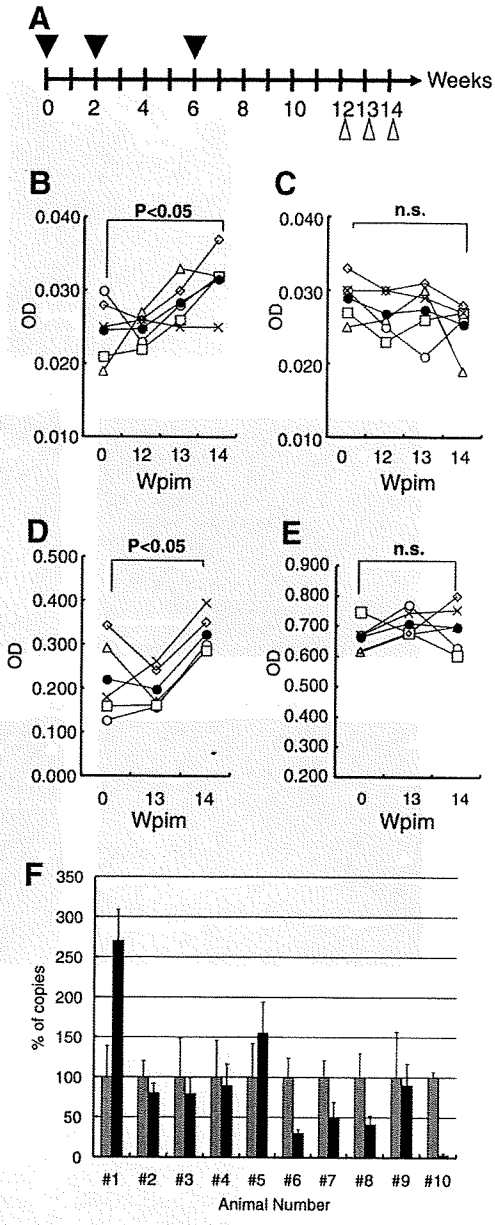

FIGURE 4. Oral immunization schedule and detection of anti-BSA or anti-rcDDR5 Abs in rhesus macaques. *A*, Immunization schedule for rhesus macaques. Five rhesus macaques (no. 6–10) were orally immunized at 0, 2, and 6 wk with TGDK-conjugated multiantigens. Another five macaques (no. 1–5) were immunized with the control Ag. Stool sampling was performed at 12, 13, and 14 wpim. Stool samples (1/10 dilution) obtained after immunization with TGDK-conjugated multiantigen (*B*; macaque no. 6 (○), 7 (△), 8 (■), 9 (◇), and 10 (×)) or control Ag (*C*; macaque no. 1 (○), 2 (△), 3 (■), 4 (◇), and 5(×)) were examined to investigate whether the anti-BSA mucosal IgA (*B* and *C*) or anti-rcDDR5 mucosal IgA (*D* and *E*) can be raised in rhesus macaques by anti-BSA ELISA and the rcDDR5-coupled multipin ELISA, as described in *Materials and Methods*. ○, Show the average OD values. *F*, Furthermore, the inhibitory effect of the stool samples from vaccinated (no. 6–10) and control groups (no. 1–5) on in vitro SIV infection was also investigated, as described in *Materials and Methods*. Percentage of copies in HSC-F infected with SIVmac239 in the presence of the 14-wpim stool sample (■) is expressed relative to that in the presence of the 0-wpim stool sample (▨), which is considered 100%.

Internalization of TGDK by PP M cells

To investigate whether rhesus macaque PP M cells can specifically take up TGDK, the rhesus macaque ileum was inoculated with FITC-labeled TGDK and subjected to immunofluorescence

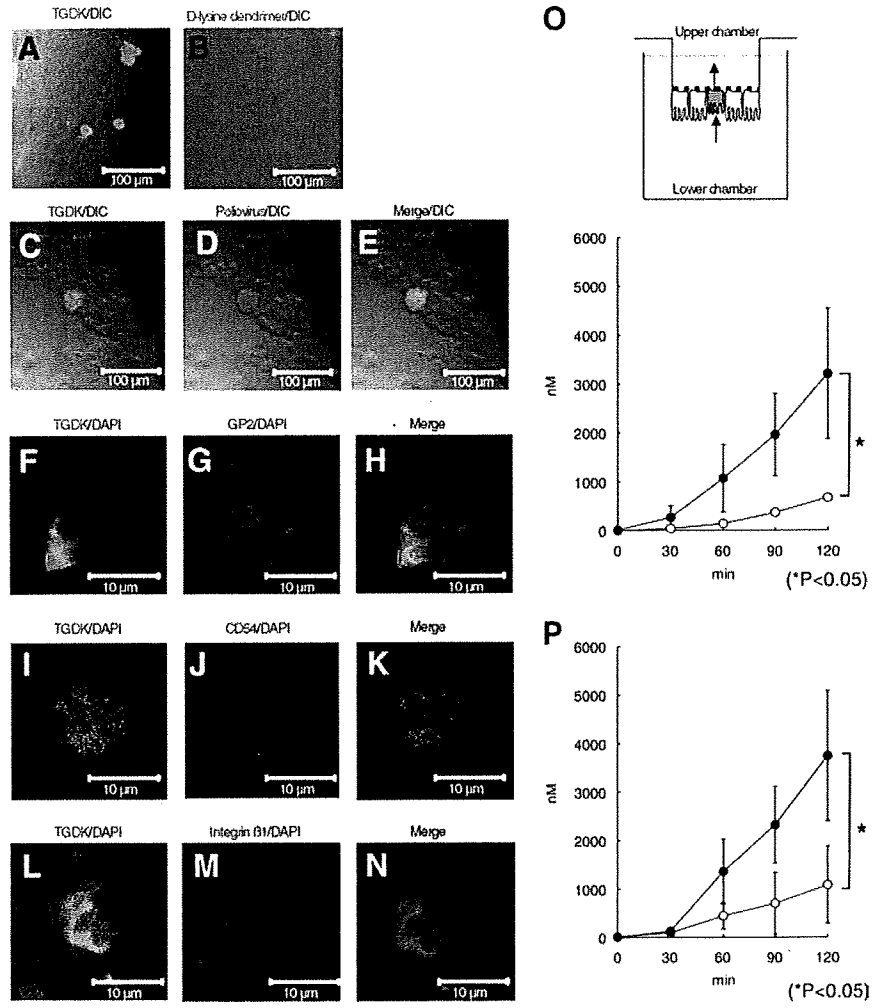

FIGURE 5. Association of TGDK with human M-like cells and transcytosis of TGDK. The Caco-2/Raji B monolayer was stained with FITC-labeled TGDK (*A*, *C*, *F*, *I*, and *L*, green) or the FITC-labeled D-lysine dendrimer (*B*, green), as described in *Materials and Methods*. Because it is known that PV can bind to M-like cells, the Caco-2/Raji B monolayer was labeled with an anti-PV Ab (*D*, red). The monolayer was further labeled with mAbs (anti-gp2 (*G*), anti-CD54 (*J*), and anti-integrin β_1 Abs (*M*), red). *A* and *C*, Show the merge image of DIC and a fluorescence image of FITC-labeled TGDK. *B*, Shows the merge image of DIC and a fluorescence image of FITC-labeled D-lysine dendrimer. *D*, Shows the merge image of DIC and a fluorescence image of monolayer labeled with an anti-PV Ab. *F*, *I*, and *L*, Show the patterns of double fluorostaining for TGDK/DAPI. *G*, *J*, and *M*, Show the patterns of double fluorostaining for gp2/DAPI, CD54/DAPI, and integrin β_1/DAPI. Furthermore, merged (*E*, *H*, *K*, and *N*) images are shown. *O*, To investigate the transcytosis activity of TGDK, the monolayers including M-like cells (●) or Caco-2 control monolayers (○) were incubated with FITC-labeled TGDK. *P*, To investigate the transcytosis efficacy of TGDK, the monolayers including M-like cells were incubated with FITC-labeled TGDK (●) or FITC (○). FITC-labeled TGDK or FITC transported from the lower chamber to the upper chamber was quantified by a CORONA Multi Microplate Reader.

analysis (Fig. 3). Recently, Terahara et al. (38) reported that gp2 is specifically expressed at a high level in mouse PP M cells. However, the expression of gp2 in rhesus PP M cells remains to be clarified in rhesus macaque. Sicinski et al. (39) reported that PV is found specifically adhering to the surface projections of M cells and in vesicles in M cells. Fig. 3*A* shows a typical TEM image of PP M cells. As expected, PV was transcytosed through typical intestinal rhesus PP M cells (Fig. 3*B*). Therefore, we confirmed whether gp2 was expressed in rhesus PP M cells, in which PV was transcytosed. Immunofluorescence analysis demonstrated that gp2 was expressed in rhesus PP M cells (Fig. 3*D*), which were recognized by the anti-PV Ab (Fig. 3*C*). These results indicated that gp2 was expressed in rhesus PP M cells. To further investigate whether TGDK specifically binds to PP M cells, the localization of TGDK was confirmed by counterstaining with the anti-gp2 Ab. As shown in Fig. 3, *F* and *G*, TGDK was colocalized with gp2. These results indicated that TGDK specifically binds to rhesus M cells.

To investigate whether TGDK is transcytosed through PP M cells, the rhesus macaque ileum was inoculated with gold-labeled TGDK and subjected to EDS (Fig. 3). The advantage of EDS is that gold-labeled TGDK can be directly detected when TGDK is completely embedded in an ultrathin section. The characteristic x-ray peak from gold (AuL-α: ~9.712 keV) is used to confirm the presence of nano-gold particles in the cytoplasm of a PP M cell within a section (Fig. 3*I*). EDS demonstrated the presence of gold-labeled TGDK in the cytoplasm of a PP M cell (*spot C*; Fig. 3, *J* and *K*), but not in the cytoplasm of a lymphocyte within a PP M cell (*spot D*; Fig. 3, *J* and *L*). In contrast, gold-labeled TGDK was not detected in intestinal epithelial cells in FAE of PPs. Taken together, these results indicate that inoculation of TGDK into the rhesus macaque ileum containing PPs shows the clear targeting of M cells and transcytosis of TGDK, and rhesus macaque PP M cells have the ability to take up TGDK from the lumen.

Immunization of rhesus macaques with TGDK-conjugated multiantigens and induction of BSA- and rcDDR5-specific Abs

To examine the in vivo effect of TGDK on M cell targeting in nonhuman primates, five rhesus macaques were immunized with TGDK-conjugated multiantigens containing BSA and rcDDR5 by oral administration according to the time schedule shown in Fig. 4*A*. Another five rhesus macaques were immunized with the control Ag. Although BSA-specific IgA in stool samples was significantly induced in the group immunized with TGDK-conjugated multiantigens at 14 wpim (Fig. 4*B*; $p < 0.05$ in repeated measures ANOVA), the immunization with the TGDK-conjugated multiantigen unfortunately induced only weak anti-BSA Ab responses. The result suggests that the induction of a stronger anti-BSA Ab response may be required for a higher content of BSA in the TGDK-conjugated multiantigen. In contrast, the immunization of rhesus macaques with the control Ag did not induce BSA-specific IgA in stool samples (Fig. 4*C*).

Our previous studies demonstrated that the rhesus macaque antisera raised against cDDR5 mimicking the conformation-specific domain of human CCR5 reacted with both human and macaque CCR5s, and potently suppressed infection by the R5 HIV-1 laboratory isolate (HIV_{JRFL}), R5 HIV-1 primary isolates (clade

A:$HIV_{93RW004}$ and clade C:HIV_{MJ4}), and a pathogenic $SHIV_{SF162P3}$ bulk isolate in vitro (29). In addition, our recent data demonstrate that mouse anti-rcDDR5-specific IgG can inhibit in vitro SIV infection (40). Therefore, the stool samples from the group immunized with TGDK-conjugated multiantigens were also examined by rcDDR5-coupled multipin ELISA to determine whether rcDDR5-specific mucosal IgA was induced. As shown in Fig. 4*D*, rcDDR5-specific IgA in stool samples was significantly induced in the group immunized with TGDK-conjugated multiantigens. In contrast, the immunization of rhesus macaques with the control Ag did not induce rcDDR5-specific IgA in stool samples (Fig. 4*E*). Although we investigated whether rcDDR5-specific mucosal IgM or IgG was also induced, the rcDDR5-specific IgM or IgG in stool samples was not significantly induced (data not shown). To further assess neutralizing activity, we performed an in vitro neutralization assay using SIVmac239. Interestingly, neutralizing activity tended to increase with the titer of the anti-rcDDR5 IgA in stool samples (Fig. 4*F*). These data suggest that TGDK-mediated vaccine delivery system represents a potential approach to develop M cell-targeted mucosal vaccines.

Selective binding and transcytosis of TGDK in human in vitro M cell model

Although TGDK promises to be an M cell targeting molecule in nonhuman primates, it still remains unclear whether TGDK effectively targets human M cells. Kernéis et al. (32) developed an in vitro human M cell model that is useful for facilitating the design of oral vaccines and efficient mucosal drug delivery systems. Therefore, we evaluated whether TGDK selectively binds to human M-like cells and is capable of transcytosis. As shown in Fig. 5, *A* and *B*, the spotlike staining of the apical surface of epithelial cells in the model with the FITC-labeled TGDK was observed, but hardly in the model with the FITC-labeled D-lysine dendrimer. Because Sicinski et al. (39) demonstrated that PV enters the human host through intestinal M cells, we examined whether TGDK can colocalize with PV on the apical surface of the model (Fig. 5, *C—E*). Immunofluorescence analysis demonstrated that M cells in the model showed costaining of TGDK and PV. Furthermore, because human M cells express gp2, CD54, and $\alpha_5\beta_1$ integrin on their surface, the apical surface of epithelial cells in the model was also stained with the anti-gp2, anti-CD54, or anti-$\alpha_5\beta_1$ integrin Ab (Fig. 5, *G*, *J*, and *M*) (41–43). Fig. 5, *G*, *J*, and *M*, shows that gp2, CD54, and $\alpha_5\beta_1$ integrin are expressed on the apical surface. Fig. 5, *H*, *K*, and *N*, shows the patterns of triple fluorostaining for TGDK/gp2/DAPI, TGDK/CD54/DAPI, or TGDK/$\alpha_5\beta_1$ integrin/DAPI in this model.

Transcytotic activity was also monitored for 120 min at 37°C. TGDK was effectively transported at 37°C through the monolayers containing M cells, but not through control monolayers (Fig. 5*O*; $p < 0.05$ in Mann-Whitney *U* test). To further confirm TGDK-mediated Ag transport, we investigated whether FITC-labeled TGDK is more efficiently transported than FITC, which is postulated as an Ag. As shown in Fig. 5*P*, FITC-labeled TGDK is more efficiently transported than FITC ($p < 0.05$ in Mann-Whitney *U* test). These results indicate that TGDK can significantly bind to human M cells and is capable of transcytosis through M cells in inductive sites, such as PPs.

Discussion

The sexual route is the most important route of HIV transmission in heterosexuals, in which the genital tract provides the virus access to lymphoid cells. In the majority of patients, the initial acquisition of HIV involves passage of the virus across a mucosal surface. Thus, blocking HIV mucosal transmission is key to prevent HIV infection.

Some studies demonstrated that mucosal Ab responses may contribute to the apparent resistance to HIV-1 infection. The studies, in which humoral and cellular responses against HIV-1 in the vaginal secretions of women who remain uninfected despite frequent unprotected sex with HIV-1-infected partners were analyzed, indicated the presence of mucosal IgA Abs to HIV-1 (44–46). Furthermore, the second type of natural resistance is found in persons with CCR5-specific mucosal autoantibodies (47). To attempt to reproduce some of the functional aspects of this natural resistance to HIV infection, many researchers have examined various types of mucosal vaccine candidate against SIV/SHIV infection because they are capable of inducing not only the immunity at the mucosal sites of transmission, which prevents the virus from gaining entry into immune cells, but also the immunity in the systemic circulation.

Could CCR5 be an attractive target for the development of mucosal vaccines? Persons with the homozygous δ32 CCR5 mutation, a 32-bp deletion of the CCR5 gene that results in a lack of cell surface expression of CCR5, have strongly reduced susceptibility to CCR5-dependent HIV-1 infection (48–50). Furthermore, Pastori et al. (51) reported that long-lasting CCR5 internalization by anti-CCR5 Abs in a subset of long-term nonprogressors is associated with a possible protective effect against disease progression, suggesting that induction of anti-CCR5 Abs by a vaccine can reproduce the immune status in long-term nonprogressors. Our previous study demonstrated that the high induction of the anti-CCR5 Ab can suppress viral propagation during acute HIV-1 i.v. transmission in cynomolgus macaques i.p. and s.c. immunized with cDDR5 mimicking the conformation-specific domain of human CCR5 (29). In this study, rcDDR5 was synthesized to induce more specific anti-rhesus CCR5 Abs. Our recent study demonstrates that the immunization of rcDDR5-conjugated KLH induces mouse anti-rcDDR5-specific IgG that specifically binds to rhesus CCR5 and inhibits in vitro SIV infection (40). These observations suggest that CCR5 can be an attractive target for the development of mucosal vaccines. Hence, to reproduce the functional aspects found in long-term nonprogressors with CCR5-specific mucosal autoantibodies, we sought new types of vaccine delivery system for the effective delivery of rcDDR5 to mucosa-associated lymphoid tissues such as PPs, the inductive site for the induction of the Ag-specific immune response.

Lectins have been investigated for targeted Ag delivery to mucosa-associated lymphoid tissues. UEA-1 and *Aleuria aurantia* lectin have high specificity for the carbohydrate moiety α-L-fucose located on the apical membranes of mouse M cells (19, 21, 52). There have been successful efforts made in in vivo targeting in mouse M cells by conjugating UEA-1 to polymerized liposomes (33) and latex particles (53), or by coating poly(D, L-lactide-co-glycolide) particles with the *A. aurantia* lectin (52). However, lectins are of limited value in vaccine delivery owing to their toxicity to humans or sensitivity to intestinal degradation. To overcome these limitations, SMPDs that appear to have high affinity for the fucose receptor on murine M cells were identified from a high-throughput screening of mixture-based compound libraries in a competitive UEA-1-binding assay (26). Although SMPDs may have the potential in oral vaccine targeting in mouse model, it remained unclear whether SMPDs effectively target nonhuman and human M cells.

The macaque model serves several important purposes in current HIV vaccine research. It allows analysis of vaccine safety and proof of immunogenicity in a species more closely related to humans. Furthermore, there are a few interesting options for testing

the effect of a vaccine on a mucosal pathogenic challenge system, such as SIV or SHIV challenges. Therefore, we investigated the M cell targeting potential of a tetragalloyl derivative, TGDK, in an in vivo nonhuman primate model. Our findings suggest that TGDK can serve as a useful targeting molecule for nonhuman primate M cells (Fig. 3). Interestingly, TGDK accumulated in GCs after it transcytosed through M cells from the gut lumen (Fig. 2, *D–F*). Although the mechanism underlying the behavior of TGDK in PP still remains to be elucidated, the ability of TGDK to accumulate in GCs may increase the possibility of interaction of an immunogen, in the form of an immune complex trapped on follicular dendritic cells, with GC B cells.

To assess the efficiency of TGDK as a mucosal delivery system, it is important to examine whether rcDDR5-specific Abs in mucosal secretions are induced in nonhuman primate models. It is generally difficult to induce a long-lasting anti-CCR5 Ab response because CCR5 is continuously exposed to the immune system. Our previous study showed that immunization with cDDR5-MAP induces anti-CCR5 serum production for ~15 wk after the third immunization, although the titer of anti-CCR5 sera declined over time until 21 wpim (29), suggesting that cDDR5-MAP is not suitable as a model Ag for the estimation of TGDK owing to its weak immunogenicity. Therefore, we introduced BSA as a standard model Ag into TGDK-conjugated multiantigens with rcDDR5 via the Hubantigen to estimate the efficiency of TGDK. Furthermore, our recent data indicate that anti-rcDDR5 serum is produced for more than 56 wk when rhesus macaques were inguinally immunized with the TGDK-conjugated multiantigens containing rcDDR5 and BSA without a specific adjuvant (our unpublished data), suggesting that the immunogenicity of TGDK-conjugated multiantigens used to evaluate the effect of TGDK was improved. Five animals were orally immunized with the TGDK-conjugated multiantigen (vaccinated group), and another five were immunized with the Hubantigen and BSA only (control group). Although the immunization with the TGDK-conjugated multiantigen induced only weak anti-BSA Ab responses in the vaccinated group (Fig. 4*B*; $p < 0.05$), rcDDR5-specific IgA in stool samples was significantly induced in the vaccinated group, as shown in Fig. 4*D*. Furthermore, the neutralizing activity tended to increase with the titer of the anti-rcDDR5 Ab in the stool samples (Fig. 4*F*). Taken together, these results show that TGDK is useful for inducing rcDDR5-specific mucosal IgA responses with neutralizing activity, although it is necessary to re-examine the dose of the orally administered TGDK-conjugated multiantigens for the perfect reproduction of the functional aspects found in long-term nonprogressors with CCR5-specific mucosal autoantibodies.

Finally, we examined whether TGDK can be available for human use using the human in vitro M cell model. Giannasca et al. (54) reported that the UEA-1 receptor is not expressed in human PPs, whereas Sharma et al. (55) reported that the UEA-1 binding was observed in M cells of human FAE. Because it further remained unclear whether the binding receptor of UEA-1 is completely the same as that of TGDK, we examined whether TGDK was directly capable of binding to human M-like cells. As shown in Fig. 5, TGDK can specifically bind to human M-like cells and transcytose through M-like cells. These results suggest that the TGDK-mediated vaccine delivery system can be available for mucosal vaccine delivery in humans.

Acknowledgments

We thank Dr. H. Matsunaga (Kumamoto University) for excellent technical assistance in TGDK synthesis. We thank K. Matsuda (Keyence) for excellent technical assistance in immunofluorescence analysis. We thank K. Nozaki, Y. Kudo, H. Kai, and K. Matsuura for excellent technical assistance in in vitro experiments.

Disclosures

The authors have no financial conflict of interest.

References

1. Pope, M., and A. T. Haase. 2003. Transmission, acute HIV-1 infection and the quest for strategies to prevent infection. *Nat. Med.* 9: 847–852.
2. Lackner, A. A., and R. S. Veazey. 2007. Current concepts in AIDS pathogenesis: insights from the SIV/macaque model. *Annu. Rev. Med.* 58: 461–476.
3. Li, Q., L. Duan, J. D. Estes, Z. M. Ma, T. Rourke, Y. Wang, C. Reilly, J. Carlis, C. J. Miller, and A. T. Haase. 2005. Peak SIV replication in resting memory $CD4^+$ T cells depletes gut lamina propria $CD4^+$ T cells. *Nature* 434: 1148–1152.
4. Guadalupe, M., E. Reay, S. Sankaran, T. Prindiville, J. Flamm, A. McNeil, and S. Dandekar. 2003. Severe $CD4^+$ T-cell depletion in gut lymphoid tissue during primary human immunodeficiency virus type 1 infection and substantial delay in restoration following highly active antiretroviral therapy. *J. Virol.* 77: 11708–11717.
5. Mascola, J. R., G. Stiegler, T. C. VanCott, H. Katinger, C. B. Carpenter, C. E. Hanson, H. Beary, D. Hayes, S. S. Frankel, D. L. Birx, and M. G. Lewis. 2000. Protection of macaques against vaginal transmission of a pathogenic HIV-1/SIV chimeric virus by passive infusion of neutralizing antibodies. *Nat. Med.* 6: 207–210.
6. Belyakov, I. M., B. Moss, W. Strober, and J. A. Berzofsky. 1999. Mucosal vaccination overcomes the barrier to recombinant vaccinia immunization caused by preexisting poxvirus immunity. *Proc. Natl. Acad. Sci. USA* 96: 4512–4517.
7. Gherardi, M. M., E. Perez-Jimenez, J. L. Najera, and M. Esteban. 2004. Induction of HIV immunity in the genital tract after intranasal delivery of a MVA vector: enhanced immunogenicity after DNA prime-modified vaccinia virus Ankara boost immunization schedule. *J. Immunol.* 172: 6209–6220.
8. Douce, G., V. Giannelli, M. Pizza, D. Lewis, P. Everest, R. Rappuoli, and G. Dougan. 1999. Genetically detoxified mutants of heat-labile toxin from *Escherichia coli* are able to act as oral adjuvants. *Infect. Immun.* 67: 4400–4406.
9. Belyakov, I. M., S. A. Hammond, J. D. Ahlers, G. M. Glenn, and J. A. Berzofsky. 2004. Transcutaneous immunization induces mucosal CTLs and protective immunity by migration of primed skin dendritic cells. *J. Clin. Invest.* 113: 998–1007.
10. Kang, S. M., Q. Yao, L. Guo, and R. W. Compans. 2003. Mucosal immunization with virus-like particles of simian immunodeficiency virus conjugated with cholera toxin subunit B. *J. Virol.* 77: 9823–9830.
11. Guo, L., X. Lu, S. M. Kang, C. Chen, R. W. Compans, and Q. Yao. 2003. Enhancement of mucosal immune responses by chimeric influenza HA/SHIV virus-like particles. *Virology* 313: 502–513.
12. Sakaue, G., T. Hiroi, Y. Nakagawa, K. Someya, K. Iwatani, Y. Sawa, H. Takahashi, M. Honda, J. Kunisawa, and H. Kiyono. 2003. HIV mucosal vaccine: nasal immunization with gp160-encapsulated hemagglutinating virus of Japan-liposome induces antigen-specific CTLs and neutralizing antibody responses. *J. Immunol.* 170: 495–502.
13. Wang, X., D. M. Hone, A. Haddad, M. T. Shata, and D. W. Pascual. 2003. M cell DNA vaccination for CTL immunity to HIV. *J. Immunol.* 171: 4717–4725.
14. Holmgren, J., C. Czerkinsky, K. Eriksson, and A. Mharandi. 2003. Mucosal immunization and adjuvants: a brief overview of recent advances and challenges. *Vaccine* 21(Suppl. 2): S89–S95.
15. Kraehenbuhl, J. P., and M. R. Neutra. 2000. Epithelial M cells: differentiation and function. *Annu. Rev. Cell. Dev. Biol.* 16: 301–332.
16. Jepson, M. A., M. A. Clark, N. Foster, C. M. Mason, M. K. Bennett, N. L. Simmons, and B. H. Hirst. 1996. Targeting to intestinal M cells. *J. Anat.* 189: 507–516.
17. Clark, M. A., M. A. Jepson, and B. H. Hirst. 1995. Lectin binding defines and differentiates M-cells in mouse small intestine and caecum. *Histochem. Cell Biol.* 104: 161–168.
18. Jepson, M. A., C. M. Mason, M. A. Clark, N. L. Simmons, and B. H. Hirst. 1995. Variations in lectin binding properties of intestinal M cells. *J. Drug Target* 3: 75–77.
19. Clark, M. A., M. A. Jepson, N. L. Simmons, T. A. Booth, and B. H. Hirst. 1993. Differential expression of lectin-binding sites defines mouse intestinal M-cells. *J. Histochem. Cytochem.* 41: 1679–1687.
20. Clark, M. A., M. A. Jepson, N. L. Simmons, and B. H. Hirst. 1995. Selective binding and transcytosis of *Ulex europaeus I* lectin by mouse Peyer's patch M-cells in vivo. *Cell Tissue Res.* 282: 455–461.
21. Giannasca, P. J., K. T. Giannasca, P. Falk, J. I. Gordon, and M. R. Neutra. 1994. Regional differences in glycoconjugates of intestinal M cells in mice: potential targets for mucosal vaccines. *Am. J. Physiol.* 267: G1108–G1121.
22. Gebert, A., and W. Posselt. 1997. Glycoconjugate expression defines the origin and differentiation pathway of intestinal M-cells. *J. Histochem. Cytochem.* 45: 1341–1350.
23. Manocha, M., P. C. Pal, K. T. Chitralekha, B. E. Thomas, V. Tripathi, S. D. Gupta, R. Paranjape, S. Kulkarni, and D. N. Rao. 2005. Enhanced mucosal and systemic immune response with intranasal immunization of mice with HIV peptides entrapped in PLG microparticles in combination with *Ulex europaeus-I* lectin as M cell target. *Vaccine* 23: 5599–5617.
24. Wang, X., I. Kochetkova, A. Haddad, T. Hoyt, D. M. Hone, and D. W. Pascual. 2005. Transgene vaccination using *Ulex europaeus agglutinin I* (UEA-1) for targeted mucosal immunization against HIV-1 envelope. *Vaccine* 23: 3836–3842.

25. Wu, Y., X. Wang, K. L. Csencsits, A. Haddad, N. Walters, and D. W. Pascual. 2001. M cell-targeted DNA vaccination. *Proc. Natl. Acad. Sci. USA* 98: 9318–9323.
26. Lambkin, I., C. Pinilla, C. Hamashin, L. Spindler, S. Russell, A. Schink, R. Moya-Castro, G. Allicotti, L. Higgins, M. Smith, et al. 2003. Toward targeted oral vaccine delivery systems: selection of lectin mimetics from combinatorial libraries. *Pharm. Res.* 20: 1258–1266.
27. Takahashi, Y., S. Misumi, A. Muneoka, M. Masuyama, H. Tokado, K. Fukuzaki, N. Takamune, and S. Shoji. 2008. Nonhuman primate intestinal villous M-like cells: an effective poliovirus entry site. *Biochem. Biophys. Res. Commun.* 368: 501–507.
28. Misumi, S., R. Nakajima, N. Takamune, and S. Shoji. 2001. A cyclic dodecapeptide-multiple-antigen peptide conjugate from the undecapeptidyl arch (from Arg^{168} to Cys^{178}) of extracellular loop 2 in CCR5 as a novel human immunodeficiency virus type 1 vaccine. *J. Virol.* 75: 11614–11620.
29. Misumi, S., D. Nakayama, M. Kusaba, T. Iiboshi, R. Mukai, K. Tachibana, T. Nakasone, M. Umeda, H. Shibata, M. Endo, et al. 2006. Effects of immunization with CCR5-based cycloimmunogen on simian/HIVSF162P3 challenge. *J. Immunol.* 176: 463–471.
30. Gibellini, D., F. Vitone, E. Gori, M. La Placa, and M. C. Re. 2004. Quantitative detection of human immunodeficiency virus type 1 (HIV-1) viral load by SYBR green real-time RT-PCR technique in HIV-1 seropositive patients. *J. Virol. Methods* 115: 183–189.
31. Ui, M., T. Kuwata, T. Igarashi, K. Ibuki, Y. Miyazaki, I. L. Kozyrev, Y. Enose, T. Shimada, H. Uesaka, H. Yamamoto, et al. 1999. Protection of macaques against a SHIV with a homologous HIV-1 Env and a pathogenic SHIV-89.6P with a heterologous Env by vaccination with multiple gene-deleted SHIVs. *Virology* 265: 252–263.
32. Kernéis, S., A. Bogdanova, J. P. Kraehenbuhl, and E. Pringault. 1997. Conversion by Peyer's patch lymphocytes of human enterocytes into M cells that transport bacteria. *Science* 277: 949–952.
33. Clark, M. A., H. Blair, L. Liang, R. N. Brey, D. Brayden, and B. H. Hirst. 2001. Targeting polymerized liposome vaccine carriers to intestinal M cells. *Vaccine* 20: 208–217.
34. Hamashin, C., L. Spindler, S. Russell, A. Schink, I. Lambkin, D. O'Mahony, R. Houghten, and C. Pinilla. 2003. Identification of novel small-molecule *Ulex europaeus I* mimetics for targeted drug delivery. *Bioorg. Med. Chem.* 11: 4991–4997.
35. Veazey, R. S., M. Rosenzweig, D. E. Shvetz, D. R. Pauley, M. DeMaria, L. V. Chalifoux, R. P. Johnson, and A. A. Lackner. 1997. Characterization of gut-associated lymphoid tissue (GALT) of normal rhesus macaques. *Clin. Immunol. Immunopathol.* 82: 230–242.
36. Dustin, M. L., R. Rothlein, A. K. Bhan, C. A. Dinarello, and T. A. Springer. 1986. Induction by IL 1 and interferon-γ: tissue distribution, biochemistry, and function of a natural adherence molecule (ICAM-1). *J. Immunol.* 137: 245–254.
37. Koopman, G., H. K. Parmentier, H. J. Schuurman, W. Newman, C. J. Meijer, and S. T. Pals. 1991. Adhesion of human B cells to follicular dendritic cells involves both the lymphocyte function-associated antigen 1/intercellular adhesion molecule 1 and very late antigen 4/vascular cell adhesion molecule 1 pathways. *J. Exp. Med.* 173: 1297–1304.
38. Terahara, K., M. Yoshida, O. Igarashi, T. Nochi, G. S. Pontes, K. Hase, H. Ohno, S. Kurokawa, M. Mejima, N. Takayama, et al. 2008. Comprehensive gene expression profiling of Peyer's patch M cells, villous M-like cells, and intestinal epithelial cells. *J. Immunol.* 180: 7840–7846.
39. Sicinski, P., J. Rowinski, J. B. Warchol, Z. Jarzabek, W. Gut, B. Szczygiel, K. Bielecki, and G. Koch. 1990. Poliovirus type 1 enters the human host through intestinal M cells. *Gastroenterology* 98: 56–58.
40. Misumi, S., A. Eto, R. Mitsumata, M. Yamada, N. Takamune, and S. Shoji. 2008. Development of cell-expressed and virion-incorporated CCR5-targeted vaccine. *Biochem. Biophys. Res. Commun.* 377: 617–621.
41. Ohno, H., K. Hase, and K. Kawano. 2008. Antigen recognition, uptake and receptor on M cells. *Clin. Immunol. Allergol.* 19: 1–9.
42. Ueki, T., M. Mizuno, T. Uesu, T. Kiso, and T. Tsuji. 1995. Expression of ICAM-1 on M cells covering isolated lymphoid follicles of the human colon. *Acta Med. Okayama* 49: 145–151.
43. Gullberg, E., A. V. Keita, S. Y. Salim, M. Andersson, K. D. Caldwell, J. D. Soderholm, and P. Artursson. 2006. Identification of cell adhesion molecules in the human follicle-associated epithelium that improve nanoparticle uptake into the Peyer's patches. *J. Pharmacol. Exp. Ther.* 319: 632–639.
44. Beyrer, C., A. W. Artenstein, S. Rugpao, H. Stephens, T. C. VanCott, M. L. Robb, M. Rinkaew, D. L. Birx, C. Khamboonruang, P. A. Zimmerman, et al. 1999. Epidemiologic and biologic characterization of a cohort of human immunodeficiency virus type 1 highly exposed, persistently seronegative female sex workers in northern Thailand: Chiang Mai HEPS Working Group. *J. Infect. Dis.* 179: 59–67.
45. Mazzoli, S., D. Trabattoni, S. Lo Caputo, S. Piconi, C. Ble, F. Meacci, S. Ruzzante, A. Salvi, F. Semplici, R. Longhi, et al. 1997. HIV-specific mucosal and cellular immunity in HIV-seronegative partners of HIV-seropositive individuals. *Nat. Med.* 3: 1250–1257.
46. Kaul, R., D. Trabattoni, J. J. Bwayo, D. Arienti, A. Zagliani, F. M. Mwangi, C. Kariuki, E. N. Ngugi, K. S. MacDonald, T. B. Ball, et al. 1999. HIV-1-specific mucosal IgA in a cohort of HIV-1-resistant Kenyan sex workers. *AIDS* 13: 23–29.
47. Barassi, C., A. Lazzarin, and L. Lopalco. 2004. CCR5-specific mucosal IgA in saliva and genital fluids of HIV-exposed seronegative subjects. *Blood* 104: 2205–2206.
48. Dean, M., M. Carrington, C. Winkler, G. A. Huttley, M. W. Smith, R. Allikmets, J. J. Goedert, S. P. Buchbinder, E. Vittinghoff, E. Gomperts, et al. 1996. Genetic restriction of HIV-1 infection and progression to AIDS by a deletion allele of the CKR5 structural gene: Hemophilia Growth and Development Study, Multicenter AIDS Cohort Study, Multicenter Hemophilia Cohort Study, San Francisco City Cohort, ALIVE Study. *Science* 273: 1856–1862.
49. Liu, R., W. A. Paxton, S. Choe, D. Ceradini, S. R. Martin, R. Horuk, M. E. MacDonald, H. Stuhlmann, R. A. Koup, and N. R. Landau. 1996. Homozygous defect in HIV-1 coreceptor accounts for resistance of some multiply-exposed individuals to HIV-1 infection. *Cell* 86: 367–377.
50. Samson, M., F. Libert, B. J. Doranz, J. Rucker, C. Liesnard, C. M. Farber, S. Saragosti, C. Lapoumeroulie, J. Cognaux, C. Forceille, et al. 1996. Resistance to HIV-1 infection in Caucasian individuals bearing mutant alleles of the CCR-5 chemokine receptor gene. *Nature* 382: 722–725.
51. Pastori, C., B. Weiser, C. Barassi, C. Uberti-Foppa, S. Ghezzi, R. Longhi, G. Calori, H. Burger, K. Kemal, G. Poli, et al. 2006. Long-lasting CCR5 internalization by antibodies in a subset of long-term nonprogressors: a possible protective effect against disease progression. *Blood* 107: 4825–4833.
52. Roth-Walter, F., I. Scholl, E. Untersmayr, R. Fuchs, G. Boltz-Nitulescu, A. Weissenbock, O. Scheiner, F. Gabor, and E. Jensen-Jarolim. 2004. M cell targeting with *Aleuria aurantia* lectin as a novel approach for oral allergen immunotherapy. *J. Allergy Clin. Immunol.* 114: 1362–1368.
53. Foster, N., M. A. Clark, M. A. Jepson, and B. H. Hirst. 1998. *Ulex europaeus I* lectin targets microspheres to mouse Peyer's patch M-cells in vivo. *Vaccine* 16: 536–541.
54. Giannasca, P. J., K. T. Giannasca, A. M. Leichtner, and M. R. Neutra. 1999. Human intestinal M cells display the sialyl Lewis A antigen. *Infect. Immun.* 67: 946–953.
55. Sharma, R., E. J. van Damme, W. J. Peumans, P. Sarsfield, and U. Schumacher. 1996. Lectin binding reveals divergent carbohydrate expression in human and mouse Peyer's patches. *Histochem. Cell Biol.* 105: 459–465.

Protein Imaging

DOI: 10.1002/anie.200903183

Fluorogenically Active Leucine Zipper Peptides as Tag–Probe Pairs for Protein Imaging in Living Cells**

*Hiroshi Tsutsumi, Wataru Nomura, Seiichiro Abe, Tomoaki Mino, Akemi Masuda, Nami Ohashi, Tomohiro Tanaka, Kenji Ohba, Naoki Yamamoto, Kazunari Akiyoshi, and Hirokazu Tamamura**

Artificial functional peptides are valuable tools in various fields of chemical biology. Small peptides, such as an oligohistidine tag (His tag), can be genetically incorporated into target proteins and used for purification of recombinant proteins, immobilization of proteins on microplates, and bioimaging of proteins on the surface of living cells with their complementary partner molecules, such as Ni^{II}–nitrilotriacetic acid complex (Ni^{II}-NTA).[1] Tsien and co-workers reported that pairs of tetracysteine motif peptides and biarsenical molecular probes, which specifically bind to tetracysteine peptides, are useful in the real-time fluorescence imaging of proteins in living cells.[2] Several pairs of other tag peptides/proteins and their specific ligands have also been reported.[3,4] In many cases, however, the bound/free (B/F) separation process of probes is necessary to avoid background emission from excess probe molecules. Fluorogenic tag–probe pairs can facilitate in distinguishing the labeled proteins from the free probes, without the B/F separation process. However, very few tag–probe pairs have been developed to date.[2a]

Engineered leucine zipper peptides, which have complementary selectivity and strong binding affinity, have been applied to tags for the affinity purification of expressed proteins, to anchors for immobilization of proteins on microplates, and to allosteric modulators of engineered enzyme activity.[5] Moreover, the hydrophobic cores of leucine zipper peptides can be engineered to form hydrophobic pockets in which small organic molecules can bind.[6] It is thought that selective binding of environmentally sensitive fluorescent dyes to these pockets inside the leucine zipper assembly might induce colorimetric changes and enhance their fluorescence intensity. The unique characteristics of leucine zipper peptides might enable production of fluorescent tag–probe pairs that are exchangeable. Herein, we describe the development of a fluorescent changeable tag–probe system based on artificial leucine zipper peptides, designated ZIP tag–probe pairs, and its application to the fluorescence imaging of ZIP tag–fused protein on the surface of living cells.

The design of ZIP tag–probe pairs is based on the crystal structure of an antiparallel coiled-coil trimer of a GCN4 mutant (Figure 1).[7] The probe peptide is an α-helical peptide with 4-nitrobenzo-2-oxa-1,3-diazole (NBD), an environmentally sensitive fluorescent dye, attached to the side chain of L-α-2,3-diaminopropionic acid, that is, Dap(NBD). Tag peptides are designed as antiparallel 2α-helical peptides linked through a Gly–Gly–Cys–Gly–Gly loop sequence. Two leucine residues, which are located at the positions complementary to the NBD in the probe peptide, are replaced by alanine or glycine so that hydrophobic pockets will be formed when the tag peptides bind to the probe peptide. Original tag peptides having two leucine residues at the complementary positions are designated as L2, and alanine- or glycine-substituted tag peptides are designated as A2 and G2, respectively.

In the UV/Vis analysis, the absorption spectra of the probe peptide changed on addition of A2 producing isosbestic points at 456, 403, and 333 nm, and thus the excitation wavelength was determined as 456 nm (Figure S1 in the Supporting Information). A fluorescence titration experiment revealed that the fluorescence spectra of the probe peptide changed remarkably with increasing A2 concentration. The emission maximum arising from the NBD dye showed a significant blue shift from 536 to 505 nm with a concurrent increase in the emission intensity (Figure 2a,b and Table 1). Such a spectral change clearly suggests that the NBD moiety of the probe peptide is located in the hydrophobic environment within the 3α-helical peptide bundle structure, which is supported by the previous report of Uchiyama et al.[8]

In the cases of L2 and G2, similar spectral changes were observed although the wavelength shifts and changes in fluorescence intensity were less than those in the case of A2 (Figure S2 in the Supporting Information and Table 1). As there is insufficient space to accommodate an NBD moiety in the complex of the L2–probe pair, the NBD moiety might bind only to the hydrophobic surface of two leucine residues of L2, thus causing the subtle fluorescence change. The

[*] S. Abe, T. Mino, A. Masuda, Prof. K. Akiyoshi, Prof. H. Tamamura
Institute of Biomaterials and Bioengineering
Tokyo Medical and Dental University
Chiyoda-ku, Tokyo 101-0062 (Japan)
and
School of Biomedical Science, Tokyo Medical and Dental University
Chiyoda-ku, Tokyo 101-0062 (Japan)
Fax: (+81) 3-5280-8036
E-mail: tamamura.mr@tmd.ac.jp
Dr. H. Tsutsumi, Dr. W. Nomura, N. Ohashi, T. Tanaka
Institute of Biomaterials and Bioengineering
Tokyo Medical and Dental University
Chiyoda-ku, Tokyo 101-0062 (Japan)
Dr. K. Ohba, Prof. N. Yamamoto
AIDS Research Center, National Institute of Infectious Diseases
Shinjuku-ku, Tokyo 162-8640 (Japan)

[**] This work was supported in part by a grant from the Naito Foundation.

Supporting information for this article is available on the WWW under http://dx.doi.org/10.1002/anie.200903183.

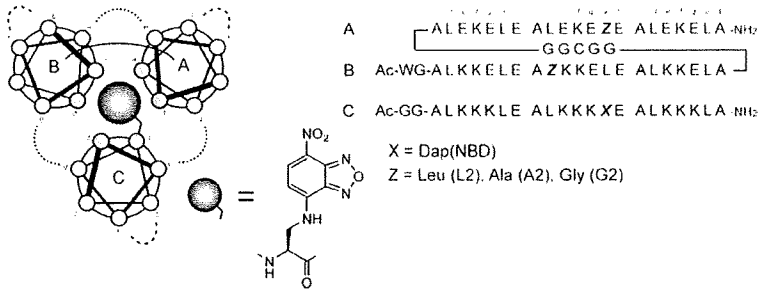

Figure 1. Structure and amino acid sequences of ZIP tag–probe pairs.

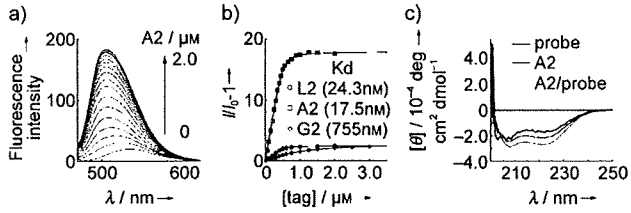

Figure 2. a) Fluorescence spectral change of the probe peptide upon addition of A2 at 25 °C in 50 mM 2-[4-(2-hydroxyethyl)piperazin-1-yl]ethanesulfonic acid (HEPES) buffer (pH 7.2, 100 mM NaCl): [probe] = 0.5 μM. b) Fluorescence titration curves of the probe peptide with L2, A2, and G2 at 516, 505, and 526 nm, respectively. I and I_0 represent the fluorescence intensity at various concentrations of tag peptides and the initial fluorescence intensity, respectively. c) Circular dichroism spectra of the A2 tag (solid line), the probe peptide (bold line), and their complex (dashed line) at 25 °C in 50 mM Tris–HCl buffer (pH 7.2, 100 mM NaCl).

Table 1: Emission maxima [nm] and $\Delta I_{max}/I_0$ values (in parentheses) of the probe peptide and tag–probe complexes, dissociation constants (K_d) [nM] between the tag and probe peptides, and the α-helix contents [%] of the probe, the tag peptides, and their complexes (in parentheses).

	Probe	L2	A2	G2
λ_{max} ($\Delta I_{max}/I_0$)	536 (–)	516 (2.7)	505 (17.9)	526 (2.5)
K_d[a]	–	24.3	17.5	755
α-helix content[b]	53	81 (78)	58 (71)	18 (41)

[a] Measurement conditions: 50 mM HEPES buffer solution (pH 7.2, 100 mM NaCl) at 25 °C, [probe] = 0.5 μM. [b] Measurement conditions: 50 mM Tris–HCl buffer solution (pH 7.2, 100 mM NaCl) at 25 °C; [tag], [probe], [tag–probe] = 1.0 μM. The α-helical contents were determined according to a standard method.[10]

wavelength shift and change in fluorescence intensity of the G2–probe pair were also small, which implies that the NBD moiety of the G2–probe peptide complex is located in a more hydrophilic area than those of the A2–probe peptide complex.

The dissociation constants of the probe peptide toward L2, A2, and G2 were estimated from the fluorescence titration curves by analysis with a nonlinear least-squares curve-fitting method[9] (Table 1). L2 and A2 showed high affinity, comparable to that of a normal antigen–antibody interaction, for the probe peptide. In general, the hydrophobicity of leucine zipper peptides is essential for their self-assembly and L2, for example, is more hydrophobic than A2 because it has two leucine residues. However, the binding affinity of the A2–probe pair is slightly superior to that of the L2–probe peptide pair, indicative not only of the hydrophobic interaction but also of the steric complementarity between A2 and the probe peptide, which is critical for the strong binding affinity. The binding affinity of G2 for the probe peptide is much lower than that of L2 or A2. Since a glycine residue generally destabilizes an α-helical structure, the structure of the G2–probe pair might be less stable than those of the L2– and A2–probe peptide pairs.

Circular dichroism (CD) spectra revealed that L2 and A2 tags, the probe peptide, and their complexes form α-helical structures (Figure 2c and Figure S3 in the Supporting Information). The probe peptide showed a CD spectral pattern typical of α-helical structures with negative maxima at 208 and 222 nm. L2, A2, and their complexes with the probe peptide also showed CD spectral patterns typical of α-helical structures. The α-helical content of A2 is lower than that of L2, which indicates that A2 forms a less stable α-helical structure than L2. However, the α-helix content of the A2–probe complex is higher than those of A2 or the probe peptides alone, which suggests that the A2–probe pair forms a stable 3α-helical bundle structure. Furthermore, the enhanced α-helical structure of the A2–probe complex is nearly equal to that in the L2–probe complex, which indicates that A2 can form a stable 3α-helical leucine zipper structure with the probe peptide. The CD spectrum of G2, however, shows a random-coil pattern and the α-helix content of the G2–probe complex is only 41 %. These results imply that the mutation of the leucine or alanine residues to glycine causes the destabilization of the structure of G2 and of the G2–probe complex, and it is thought that this is the reason why the G2–probe pair has a lower binding affinity than the A2–probe pair.

The fluorescence titration experiment and the CD spectra suggest that formation of a stable α-helical structure with a hydrophobic pocket is necessary for high binding affinity and fluorogenic activity. A2 forms a stable α-helical structure with a pocket that can accommodate NBD and it is thought, therefore, that the combination of the A2 tag and the probe leads to expression of the remarkable fluorescence activity. In addition, the A2–probe pair showed the same fluorescence spectral change in the cell lysate solution (Figure S7 in the Supporting Information), thus indicating that A2 is the most appropriate partner of the probe peptide as a fluorogenic tag–probe pair for protein imaging in vivo.

Next, we investigated whether our ZIP tag–probe system is available for the fluorescence imaging of proteins in living cells. CXCR4 was chosen as a model protein. CXCR4 is one of the 7-transmembrane G-protein coupled receptors, a member of a chemokine receptor family.[11] The A2 tag is genetically fused at the N terminus of CXCR4, which is an extracellular region, through the $(Gly\text{-}Ser)_6$ linker sequence. The A2-tag-fused CXCR4 is transiently expressed on the surface of Chinese hamster ovary K1 (CHO-K1) cells, and double labeling experiments of the A2-tag-fused CXCR4 using a fluorescent CXCR4 antagonist with tetramethylrhod-

amine (TAMRA)[12] and the probe peptide with the NBD dye were performed. The A2-tag-fused CXCR4 was specifically stained with red fluorescence by TAMRA-appended CXCR4 antagonist (Figure S8a in the Supporting Information). Then, the sequential labeling of the A2-tag-fused CXCR4 was performed using the probe peptide. Before removal of the probe peptide, a bright green fluorescence was observed on the surface of cells in the presence of excess probe peptide, but the fluorescence resulting from this peptide was not observed in CHO-K1 cells without expression of the A2-tag-fused CXCR4 (Figure 3b). Fluorescence arising from the TAMRA-appended CXCR4 antagonist was also observed (Figure 3a), which suggests that the binding events between the A2 tag and the probe peptide, and between CXCR4 and the TAMRA-appended CXCR4 antagonist, are independent of each other. The fluorescence image derived from the probe peptide was merged well with the fluorescence image of the TAMRA-appended CXCR4 antagonist (Figure 3c,d). After removal of the probe peptide by the exchange of culture medium, similar fluorescence images were also observed (Figure S9 in the Supporting Information). These results suggest that CXCR4 can be successfully visualized using our ZIP tag–probe system without removal of excess probe molecules. This ZIP tag–probe system is consequently a useful fluorescence-imaging tool for proteins in living cells.

In conclusion, we have developed a new functional peptide pair with fluorogenic activity based on leucine zipper peptides. The alanine-substituted tag peptide A2 binds strongly to a probe peptide, and this binding is accompanied by a dramatic fluorescent colorimetric change from weak yellow to bright green. In addition, we have demonstrated that the fluorescence imaging of A2-tag-fused CXCR4, which is a membrane-bound protein, is successfully achieved by the probe peptide. Recently, Yano et al. reported that two α-helical leucine zipper tag–probe pairs are useful fluorescence imaging tools for membrane-bound proteins.[13]

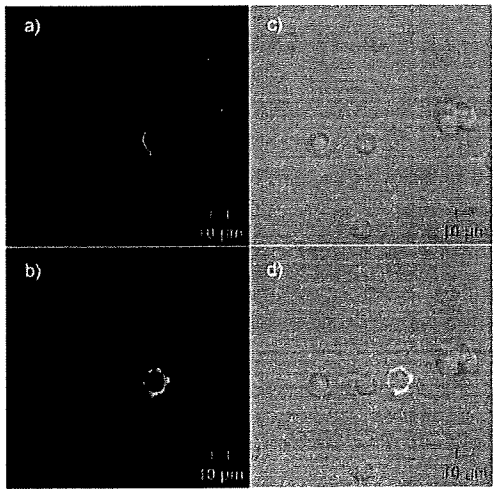

Figure 3. Sequential labeling of A2-tag-fused CXCR4 by the probe peptide after labeling by TAMRA-appended CXCR4 antagonist. a) Fluorescence image derived from TAMRA (excitation: 543 nm, emission filter: > 560 nm). b) Fluorescence image derived from NBD (excitation: 458 nm, emission filter: 505–530 nm). c) Differential interference contrast. d) Merged image of (a)–(c).

Our ZIP tag–probe pairs have, in addition, fluorogenic activity which might facilitate the real-time imaging of proteins without the necessity to remove excess probe molecules. Thus, ZIP tag–probe pairs would become valuable imaging tools for target proteins in living cells.

Received: June 12, 2009
Revised: September 24, 2009
Published online: October 28, 2009

Keywords: fluorescent probes · imaging · living cells · peptides · proteins

[1] a) K. Terpe, *Appl. Microbiol. Biotechnol.* **2003**, *60*, 523–533; b) M. Hedhammar, T. Gräslund, S. Hober, *Chem. Eng. Technol.* **2005**, *28*, 1315–1325; c) E. G. Guignet, R. Hovius, H. Vogel, *Nat. Biotechnol.* **2004**, *22*, 440–444; d) C. R. Goldsmith, J. Jaworski, M. Sheng, S. J. Lippard, *J. Am. Chem. Soc.* **2006**, *128*, 418–419; e) C. T. Hauser, R. Y. Tsien, *Proc. Natl. Acad. Sci. USA* **2007**, *104*, 3693–3697.

[2] a) B. A. Griffin, S. R. Adams, R. Y. Tsien, *Science* **1998**, *281*, 269–272; b) G. Gaietta, T. J. Deerinck, S. R. Adams, J. Bouwer, O. Tour, D. W. Laird, G. E. Sosinsky, R. Y. Tsien, M. H. Ellisman, *Science* **2002**, *296*, 503–507.

[3] a) K. M. Marks, M. Rosinov, G. P. Nolan, *Chem. Biol.* **2004**, *11*, 347–356; b) A. Ojida, K. Honda, D. Shinmi, S. Kiyonaka, Y. Mori, I. Hamachi, *J. Am. Chem. Soc.* **2006**, *128*, 10452–10459; c) I. Chen, Y.-A. Choi, A. Y. Ting, *J. Am. Chem. Soc.* **2007**, *129*, 6619–6625; d) H. M. O'Hare, K. Johnsson, A. Gautier, *Curr. Opin. Struct. Biol.* **2007**, *17*, 488–494.

[4] a) A. Keppler, S. Gendreizig, T. Gronemeyer, H. Pick, K. Johnsson, *Nat. Biotechnol.* **2003**, *21*, 86–89; b) A. Gautier, A. Juillerat, C. Heinis, I. R. Corrêa, Jr., M. Kindermann, F. Beaufils, K. Johnsson, *Chem. Biol.* **2008**, *15*, 128–136; c) J. Yin, F. Liu, X. Li, C. T. Walsh, *J. Am. Chem. Soc.* **2004**, *126*, 7754–7755; d) G. V. Los, A. Darzins, N. Karassina, C. Zimprich, R. Learish, M. G. McDougall, L. P. Encell, R. Friedman-Ohana, M. Wood, G. Vidurgiris et al., *Promega Cell Notes* **2005**, *11*, 2–6.

[5] a) B. Tripet, L. Yu, D. L. Bautista, W. Y. Wong, R. T. Irvin, R. S. Hodges, *Protein Eng.* **1996**, *9*, 1029–1042; b) K. Zhang, M. R. Diehl, D. A. Tirrell, *J. Am. Chem. Soc.* **2005**, *127*, 10136–10137; c) S. Yuzawa, T. Mizuno, T. Tanaka, *Chem. Eur. J.* **2006**, *12*, 7345–7352.

[6] a) I. Obataya, S. Sakamoto, A. Ueno, H. Mihara, *Biopolymers* **2001**, *59*, 65–71; b) M. K. Yadav, J. E. Redman, L. J. Leman, J. M. Alvarez-Gutiérrez, Y. Zhang, C. D. Stout, M. R. Ghadiri, *Biochemistry* **2005**, *44*, 9723–9732.

[7] B. Lovejoy, S. Choe, D. Cascio, D. K. McRorie, W. F. DeGrado, D. Eisenberg, *Science* **1993**, *259*, 1288–1293.

[8] S. Uchiyama, T. Santa, K. Imai, *J. Chem. Soc. Perkin Trans. 2* **1999**, 2525–2532.

[9] T. Kuwabara, A. Nakamura, A. Ueno, F. Toda, *J. Phys. Chem.* **1994**, *98*, 6297–6303.

[10] a) Y.-H. Chen, J. T. Yang, K. H. Chau, *Biochemistry* **1974**, *13*, 3350–3359; b) P. J. Gans, P. C. Lyu, M. C. Manning, R. W. Woody, N. R. Kallenbach, *Biopolymers* **1991**, *31*, 1605–1614; c) D. Y. Jackson, D. S. King, J. Chmielewski, S. Singh, P. G. Schultz, *J. Am. Chem. Soc.* **1991**, *113*, 9391–9392.

[11] a) S. G. Ward, J. Westwick, *Biochem. J.* **1998**, *333*, 457–470; b) H. Tamamura, H. Tsutsumi, W. Nomura, T. Tanaka, N. Fujii, *Expert Opin. Drug Discovery* **2008**, *3*, 1155–1166.

[12] W. Nomura, Y. Tanabe, H. Tsutsumi, T. Tanaka, K. Ohba, N. Yamamoto, H. Tamamura, *Bioconjugate Chem.* **2008**, *19*, 1917–1920.

[13] Y. Yano, A. Yano, S. Oishi, Y. Sugimoto, G. Tsujimoto, N. Fujii, K. Matsuzaki, *ACS Chem. Biol.* **2008**, *3*, 341–345.

